Differences in Electrostatic Properties at Antibody–Antigen Binding Sites: Implications for Specificity and Cross-Reactivity

Neeti Sinha, Srinivasan Mohan, Claudia A. Lipschultz, and Sandra J. Smith-Gill
Basic Research Laboratory, National Cancer Institute at Frederick, National Institutes of Health, Frederick, Maryland 21702 USA

ABSTRACT Antibodies HyHEL8, HyHEL10, and HyHEL26 (HH8, HH10, and HH26, respectively) recognize highly overlapping epitopes on hen egg-white lysozyme (HEL) with similar affinities, but with different specificities. HH8 binding to HEL is least sensitive toward mutations in the epitope and thus is most cross-reactive, HH26 is most sensitive, whereas the sensitivity of HH10 lies in between HH8 and HH26. Here we have investigated intra- and intermolecular interactions in three antibody–protein complexes: theoretical models of HH8-HEL and HH26-HEL complexes, and the x-ray crystal structure of HH10-HEL complex. Our results show that HH8-HEL has the lowest number and HH26-HEL has the highest number of intra- and intermolecular hydrogen bonds. The number of salt bridges is lowest in HH8-HEL and highest in HH26-HEL. The binding site salt bridges in HH8-HEL are not networked, and are weak, whereas, in HH26-HEL, an intramolecular salt-bridge triad at the binding site is networked to an intermolecular triad to form a pentad. The pentad and each salt bridge of this pentad are exceptionally stabilizing. The number of binding-site salt bridges and their strengths are intermediate in HH10-HEL, with an intramolecular triad. Our further calculations show that the electrostatic component contributes the most to binding energy of HH26-HEL, whereas the hydrophobic component contributes the most in the case of HH8-HEL. A "hot-spot" epitope residue Lys-97 forms an intermolecular salt bridge in HH8-HEL, and participates in the intermolecular pentad in the HH26-HEL complex. Mutant modeling and surface plasmon resonance (SPR) studies show that this hot-spot epitope residue contributes significantly more to the binding than an adjacent epitope residue, Lys-96, which does not form a salt bridge in any of the three HH-HEL complexes. Furthermore, the effect of mutating Lys-97 is most severe in HH26-HEL. Lys-96, being a charged residue, also contributes the most in HH26-HEL among the three complexes. The SPR results on these mutants also highlight that the apparent "electrostatic steering" on net on rates actually act at post-collision level stabilization of the complex. The significance of this work is the observed variations in electrostatic interactions among the three complexes. Our work demonstrates that higher electrostatics, both as a number of short-range electrostatic interactions and their contributions, leads to higher binding specificity. Strong salt bridges, their networking, and electrostatically driven binding, limit flexibilities through geometric constrains. In contrast, hydrophobic driven binding and low levels of electrostatic interactions are associated with conformational flexibility and cross-reactivity.

INTRODUCTION

Biomolecular association is proposed to occur in two steps: 1) encounter, which involves diffusion-limited orientation of the two molecules driven by nonspecific, long-range, electrostatic forces followed by collision to form a hydrophobically associated encounter complex; and 2) docking with the formation of specific contacts and noncovalent bonds (Haselkorn et al., 1974; Ross and Subramanian, 1981; Schreiber and Fersht, 1996). Electrostatic interactions would therefore be expected to directly influence the initial association, through steering, and the strength of docked complex due to electrostatic interactions of salt bridges and hydrogen bonds. Ligand binding also often induces conformational changes in both receptor and ligand during the docking step (Musci et al., 1988; Nicholson et al., 1995; Wagner 1995; Sparrer et al., 1996; Kawaguchi et al., 1997; Walters et al., 1997; Lindner et al., 1999).

Antibody–antigen complexes have long served as models to study general principals of protein–protein interactions and molecular recognition, both experimentally (Kabat et al., 1977; Smith-Gill, 1991; Wilson and Stanfield, 1993; Tsumoto et al., 1994; Braden and Poljak, 1995; Dall'Acqua et al., 1998) and computationally (Novotny et al., 1989; Chong et al., 1999; Freire, 1999). High-affinity antibodies, very specific toward their antigens (Eaton et al., 1995), or proposed to have "lock and key" type of binding (Wedemayer et al., 1997), have higher electrostatic interactions with their antigens (Chong et al., 1999). In contrast, more cross-reactive antibodies are believed to be more flexible and involve less specific contacts. It is becoming increasingly evident that flexibility may also play a major role in specificity and dynamics of high-affinity antibodies (Mian et al., 1991; Foote and Milstein 1994; Ditzel et al., 1996; Sheriff et al., 1996; Diaw et al., 1997), even in cases where crystal structures of the complexed and uncomplexed antibodies did not indicate significant induced fit (Lindner et al., 1999). Nevertheless, the functional role and the structural basis of conformational change in antibody binding

Submitted December 26, 2001 and accepted for publication August 21, 2002.

Address reprint requests to S. J. Smith-Gill, Basic Research Laboratory, NCI at Frederick, Bldg. 469, Rm 206, Frederick, MD 21702. Tel.: 301-846-5203; Fax: 301-846-6326; E-mail: smithgil@helix.nih.gov.

Dr. Mohan's present address is Protein Chem., Medarex Inc., 521 Cottonwood Dr., Milpitas, CA 95035.

0006-3495/02/12/2946/23 $2.00

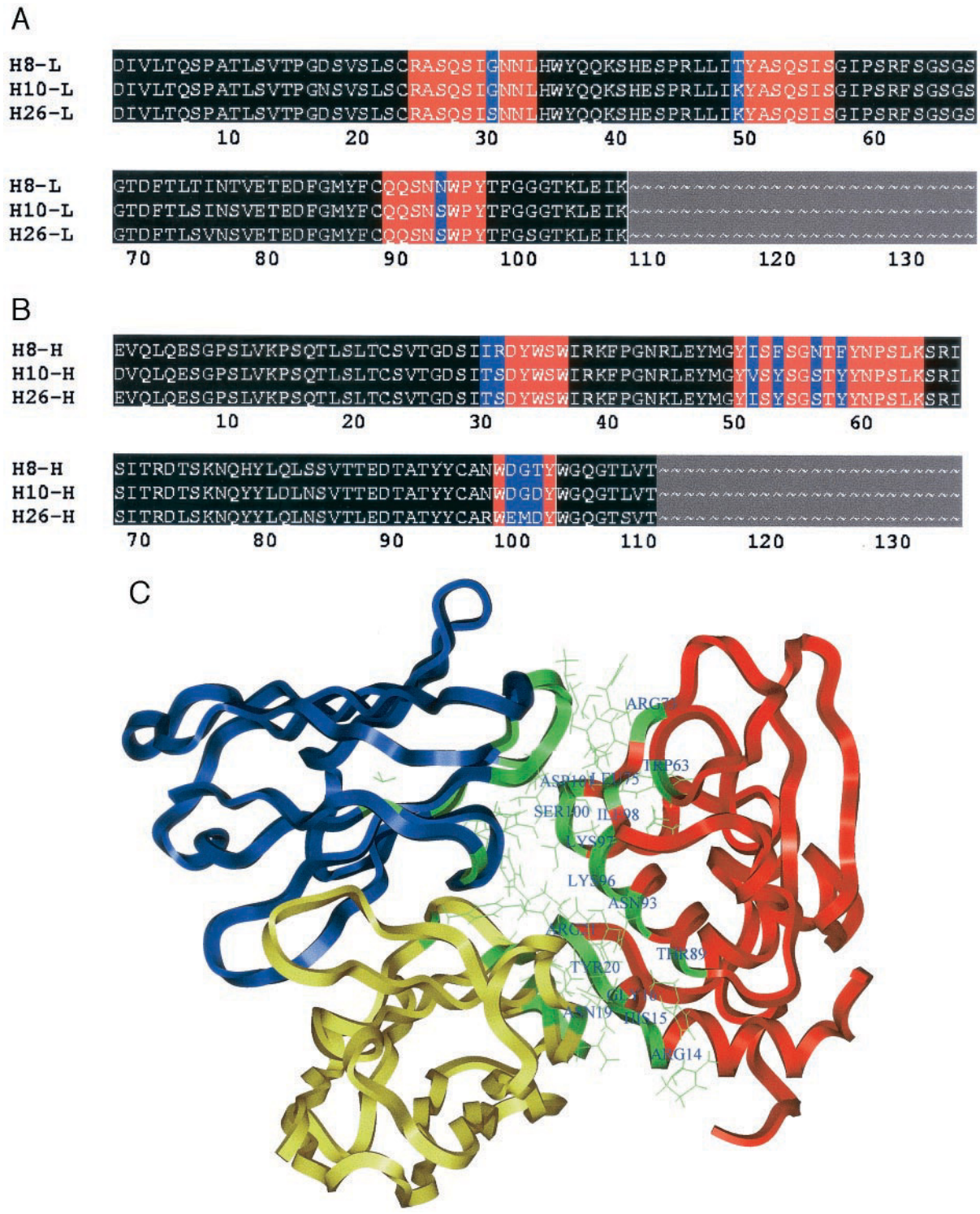

FIGURE 1 Illustration of HH antibodies structural associations with HEL. Sequence alignment of (*a*) light-chains, and (*b*) heavy-chains of HH8, HH10, and HH26 antibodies. Colored areas represent the complementarity determining regions (CDRs). Red depicts conserved residues and blue depicts substitutions. Conserved and substituted residues are only shown for CDRs. There are no insertions and deletions, and CDRs are of identical lengths (Padlan et al., 1989). The substitutions occur in CDRs and the frame work regions of the antibodies. Light chains of these antibodies are encoded from the same V_k germ line gene, while their heavy chains belong to the same family (Lavoie et al., 1992). Two charged residues, which might be playing important roles in the electrostatically driven binding, are somatically mutated to hydrophobic residues in HH8. The residue Lys-49_L, in CDR 2 of the light chain and residue Asp-101_H, in CDR 3 of the heavy chain, present in HH10 and HH26, have been mutated to threonines in HH8. These residue differences have been shown to play a role in determining the binding mechanisms of these antibodies, possibly through long range effects (Lavoie et al., 1992). Similarly, the positions of two tyrosines, Tyr-53_H and Tyr-58_H, in CDR 2 of the heavy chain in HH10 and HH26, are occupied by phenylalanines in HH8. (*c*) HH10-HEL

remains unpredictable for any given complex, and the structural and thermodynamic determinants of antibody specificity and affinity are not completely understood.

We have previously proposed that differences in fine specificity among three structurally and functionally related antibody–protein complexes reflect their relative flexibilities, which are modulated, at least in part, by intramolecular salt links and salt-link networks within the complementarity-determining regions (CDRs), and by the proportions of hydrophobic and electrostatic residues (S. Mohan and S. J. Smith-Gill, submitted). Monoclonal antibodies HyHEL8, HyHEL10 and HyHEL26 (HH8, HH10 and HH26, respectively), share more than 90% of sequence homology (Fig. 1, *a* and *b*), and are specific for similar epitopes on hen egg white lysozyme (HEL) (Newman et al., 1992; Y. Li, C. A. Lipschultz, and S. J. Smith-Gill, unpublished results) (Fig. 1 *c*), with similar affinity (Lavoie et al., 1992, 1999). The structural, functional, and physical properties of HH8, HH10, and HH26 correlate with their cross-reactivity properties, ranking HH8 at one extreme, HH26 at the other, and HH10 intermediate. Of particular interest to the present study are the varying number of intramolecular salt bridges at the binding sites, which rank HH8 $<$ HH10 $<$ HH26, and the differences in the proportion of hydrophobic residues, which rank HH8 $>$ HH10 $>$ HH26 (Smith-Gill et al., 1987; S. Mohan and S. J. Smith-Gill, submitted). Salt bridges and hydrogen bonds have important roles in protein structure and function (Perutz, 1970; Barlow and Thornton, 1983; Musafia et al., 1995; Xu et al., 1997a,b), and have been linked to protein stability (Kumar et al., 2000; Yip et al., 1998), and flexibility (Sinha et al., 2001a,b). Modification of intramolecular salt bridges in HH10 alters its cross-reactivity (Lavoie et al., 1992, 1999). Therefore, we hypothesize that, among the three antibodies, HH26 has the most rigid binding site, whereas HH8 has the most flexible binding site.

Surface plasmon resonance (SPR) analysis shows that the association kinetics of HH-HEL binding of these three complexes are best described by a two-step model (Lipschultz et al., 2000), which we interpret as an encounter followed by a docking or annealing, which may involve conformational rearrangements. The data also suggest that the energy barriers to docking are lowest in the HH8-HEL complex, highest in the HH26-HEL complex, and intermediate in HH10-HEL, especially in complexes with HEL containing epitope mutations (Li et al., 2001; S. Mohan and S. J. Smith-Gill, unpublished). Furthermore, among the three complexes, HH8-HEL derives the greatest proportion and amount of its free energy change from the docking step, HH26-HEL the least, and HH10-HEL an intermediate amount (Lipschultz et al., 2000; Li et al., 2001). Complex stability, as measured by net dissociation rates, is more sensitive to antigenic mutation in HH26 and HH10 complexes than in HH8 (Lavoie et al., 1999; Li et al., 2001). In addition, the three complexes differ in degree of sensitivity of their initial association rates to mutation, with HH8 being the least sensitive and HH26 the most (Lavoie et al., 1999; Li et al., 2001; S. Mohan and S. J. Smith-Gill, unpublished).

Here we utilize a combination of computational and experimental methods to examine in greater detail the structural and thermodynamic properties of these three complexes, specifically testing the hypothesis that the number and strength of electrostatic interactions influence association at both intermolecular and intramolecular levels. The former contributes directly to intermolecular complementarity and free energy of binding (Sheinerman et al., 2000; Kangas and Tidor, 2001), and the latter contributes indirectly to specificity and affinity by modulation of protein flexibility, or flexibility–rigidity compensations in general. Here we show that, overall, the electrostatic component dominates in HH26-HEL binding, and hydrophobicity dominates in HH8-HEL binding. We show that the number of short-range electrostatic interactions, the electrostatic strengths, and the networking pattern of binding-site salt bridges, and the overall electrostatic contributions toward binding correspond to the association properties of these antibodies. This indicates that the electrostatic properties have striking functional significance in governing the flexibility and rigidity with which protein–protein binds. We also show that electrostatic interactions can have a differential impact on the encounter and docking steps of association. These results provide an insight into the structural and thermodynamic manifestation of flexibility and rigidity.

MATERIALS AND METHODS

Antibody–antigen complexes

The coordinates for the HH10-HEL and HH10Fv-HEL complexes, and unbound HEL, were obtained from the protein data bank (PDB) (Bernstein et al., 1977) (PDB ID: HH10-HEL, 3hfm; HH10Fv-HEL, 1c08; HEL, 1bwh). HH10-HEL, HH10Fv-HEL, and unbound HEL were crystal structures at 3.0-, 2.3-, and 1.8-Å resolutions, respectively. HH8-HEL and HH26-HEL were theoretical structures, generated in this lab (S. Mohan and S. J. Smith-Gill, submitted) using "Model Homologue" module of LOOK software (Molecular Application Group) package. The module uses the algorithm "segmod" (Levitt, 1992), which homology models the target protein, using template structure, by optimizing the packing interactions between the side chains. HH10-HEL was used as a template to model HH8-HEL and HH26-HEL (S. Mohan and S. J. Smith-Gill, submitted).

(PDB ID:3hfm) is shown. Heavy chain, light chain, and HEL are shown by purple, yellow, and red, respectively. Contact epitope and paratope residues (Lavoie et al., 1999) are illustrated in green. Epitope and paratope residues are also shown by their side chains. The names and positions of epitope residues are shown. Insight II (ACCELRYS) was used to generate the picture.

Hydrogen bonds, salt bridges and buried surface area

The presence of a hydrogen bond is inferred when two nonhydrogen atoms with opposite partial charges are within a distance of 3.5 Å. Geometrical goodness of H-bonds was assessed by computing the two angles: θ_D between vectors BD–D and D–A, where BD is covalently bonded to D; and θ_A between D–A and A–BA, where BA is covalently bonded to A. Hydrogen-bonds with both the angles in the range of 90–150^o were considered to be of good geometry, and are listed here. Salt bridges are inferred upon meeting the two criteria: the centroids of the oppositely charged side-chain functional groups of charged residues (Asp, Glu, Lys, Arg, and His) are within 4.0 Å; and Aspartate or glutamate side-chain carbonyl oxygen atom is within 4.0 Å distance from nitrogen atom of arginine, lysine or histidine side chains. When, for the same pair of residues, there are more than one pair of nitrogen–oxygen atoms present within 4.0 Å, the salt bridge has been counted only once. If a salt bridge involves a CDR or an epitope residue, it is considered to be a binding-site salt bridge.

Solvent-accessible surface area is calculated with a probe radius of 1.4 Å, using the algorithm of Lee and Richards (1971). The surface area buried upon the complex formation is the difference in solvent-accessible surface area between free and bound states:

ASA of free antibody + ASA of free antigen

− ASA of antibody–antigen complex.

Hydrophobicity

The method of Chothia (1974) was followed to estimate the hydrophobic contribution to the free energy of binding. This method is based on the observation that free energy of transferring an amino-acid side chain from water to a nonpolar solvent (the hydrophobic effect) is directly proportional to the solvent-accessible surface area of the side chains (Rose et al., 1985), where 1 Å^2 of buried surface corresponds to 25 cal of hydrophobic stabilization. Buried surface area upon complex formation was calculated as described above. The hydrophobic contribution was calculated as ΔG_{hydro} (kcal/mol) = (Area buried upon the complex formation × 25) ÷ 1000.

Electrostatic contributions of salt bridges

We have computed the electrostatic strength of salt bridges using a continuum electrostatic approach to solve the linearized Poisson–Boltzmann equation, using the DELPHI computer program developed by Honig and co-workers (Gilson et al., 1985; Gilson and Honig, 1987). The method has been widely used (Hendsch and Tidor, 1994; Xu et al., 1997a; Lounnas and Wade, 1997; Sinha et al., 2001a) and experimentally supported (Waldburger et al., 1995, 1996). The electrostatic contribution of a salt bridge to the free energy of folding is calculated as described by Hendsch and Tidor (1994). The electrostatic strength of a salt bridge is measured relative to computer mutation of salt-bridging side chains to their hydrophobic isosters. A hydrophobic isoster is the salt-bridging side chain with its partial atomic charges set to zero (Hendsch and Tidor, 1994). Side chain alone in solution was used for the unfolded state, which was therefore used as a reference state. The electrostatic contributions of salt bridges are calculated for folded state, as compared to the unfolded state. The electrostatic strength of a salt bridge can be divided into three component terms: $\Delta\Delta G_{desol}$, the sum of the charge desolvation penalties paid by the salt-bridging side chains, when they are brought from the dielectric of 80.0 (in water) to the dielectric of 4.0 (in the protein interior); $\Delta\Delta G_{bridge}$, the favorable energy change due to electrostatic interaction between opposite charges of salt-bridging side chains; and $\Delta\Delta G_{protein}$, electrostatic interactions of salt-bridging side chains with the charges in the rest of the protein. The total electrostatic energy upon the salt-bridge formation would be

$$\Delta\Delta G_{tot} = \Delta\Delta G_{desol} + \Delta\Delta G_{bridge} + \Delta\Delta G_{protein}. \quad (1)$$

The DELPHI software package calculates the electrostatic potential in and around macromolecules, using the iterative finite difference solution to the Poisson–Boltzmann equation. The desolvation penalty, bridge term, and protein term were calculated as described by Hendsch and Tidor (1994). The desolvation penalty of a salt-bridging side chain upon protein folding was computed by setting the partial charges of all atoms, except ones in the salt-bridging side chain, to 0. The reaction field energy was calculated for each salt-bridging side chain, with its respective partial charges on. The charge desolvation was computed similarly in the unfolded state. Thus, in the unfolded model, the salt-bridging side chains are present in solvent, and are infinitely separated from each other. The coordinates for salt-bridging side chains are taken from x-ray structure, and, for unfolded-state calculation, these were placed at exactly the same position on the finite-difference grid as they occupy in the folded state. For each of the salt-bridging side chains, the reaction field energy in the unfolded state was subtracted from the reaction field energy in the folded state to give the charge desolvation penalty. The sum of the charge desolvation penalties of both side chains is the charge desolvation penalty of the salt bridge, $\Delta\Delta G_{desol}$.

For electrostatic interactions between salt-bridging side chains, the linearized Poisson–Boltzmann equation was solved after setting all the partial charges of the molecule to 0, except those on one of the salt-bridging side chains. The potential at each partial charge position on the other side chain was determined to estimate the bridge term,

$$\Delta\Delta G_{Bridge} = \sum_i \phi iqi, \quad (2)$$

where ϕ is the potential, and q is magnitude at i partial charge of the other side chain.

The contribution due to charge interactions between salt-bridging side chains and the rest of the protein is estimated by solving the Poisson–Boltzmann equation in the folded state, with atomic charges, except for those in salt-bridging side chains, set to 0. The protein term, $\Delta\Delta G_{Protein}$, is calculated as

$$\Delta\Delta G_{Protein} = \sum_i \phi iqi, \quad (3)$$

where i ranges over all partial charges in whole protein, excluding charged atoms of salt-bridging side chains.

The strength of pentad and triad salt-bridge networks were computed considering each as a unit. The electrostatic strength of the salt-bridge network was computed similarly, by taking into account the charge desolvation penalty of all interacting side chains, all possible electrostatic interactions and the protein term. A salt-bridge network will have favorable and unfavorable interactions, between opposite and like charges, respectively.

The protein structure was mapped on 79 × 79 × 79 point 3-dimensional grid for iterative finite difference calculations. The grid spacing was kept 0.83 Å. Hydrogen atoms were added to the structures, and the protonation state of the charged residues were defined at pH 7.0, using the BIOPOLYMER module of INSIGHT II (ACCELRYS). PARSE3 set of atomic charges and radii (Sitkoff et al., 1994) were used, with a solvent probe radius of 1.4 Å. The dielectric constant of solute (protein) was kept at 4.0 and that of solvent was kept at 80.0. The ionic strength of 145 mM was used to simulate the physiological conditions. The output energy value in units kT, where k is the Boltzman constant and T is the absolute temperature, were multiplied with the conversion factor 0.592 to obtain the results in kilo-calories per mole at the room temperature, 25°C. For each calculation, the structures were first mapped on the grid where the molecule occupied 50% of the grid and Debye–Huckel boundary conditions were

applied (Klapper et al., 1986). The resulting rough calculations were used as a boundary condition for focused calculation, where molecule extent was kept 95% on the grid. The results of focused calculations are shown here.

Electrostatic contribution to antibody antigen binding

The electrostatic contributions are calculated as the sum of charge desolvation penalties paid by antibody and antigen upon complex formation plus their electrostatic interactions. The electrostatic contributions were calculated for bound state, compared to the unbound. The reference state used here was unbound state. The continuum electrostatic approach was used to solve the linearized Poisson–Boltzmann equation, by means of the finite difference method, as described above, using DELPHI software.

Point mutation

Structures with alanine mutations were generated using the "Mutant Modeling" module of the software package LOOK3.0 (Molecular Applications Group, Palo Alto, CA). This module used an algorithm 'cara' (Lee and Subbiah, 1991), which models the side-chain conformation of substituted residues and the residues with which it contacts. The method applies the simulated annealing algorithm to optimize side-chain Van der Waals interactions. The predictions using this method have been shown to be accurate, particularly for nonsurface residues (Lee and Subbiah, 1991). Lysine was substituted with alanine in the sequence. This sequence was used as a new sequence to generate a model, using the original structure as template. The new mutant was used for binding energy calculations.

Binding kinetics

HEL or single-site mutants were expressed and purified in *Pichia pastoris* (Li et al., 2000, 2001), and immobilized on a CM5 sensor chip. Recombinant Fab (Li et al., 2001) was used as analyte, and the binding was monitored by SPR, using a BIAcore1000 or BIAcore2000 instrument. The rate constants for encounter (k_{+1}, k_{-1}) and docking (k_{+2}, k_{-2}) were calculated by global analysis of the binding curves, using a two-step model and BIAeval3.02 software, as described and detailed elsewhere (Lipschultz et al., 2000; Li et al., 2001), and used to calculate affinities for encounter ($Ka1 = k_{+1}/k_{-1}$), docking ($Ka2 = k_{+2}/k_{-2}$) and the total binding ($K = Ka1(1 + Ka2)$). Gibbs free energy change for each equilibrium constant (encounter, $\Delta G1$; Docking, $\Delta G2$; Total, ΔG) was calculated using the relationship: $\Delta G = -RT \ln(Ka)$. $\Delta\Delta G$, the change in free energy due to a given mutant, was calculated as:

$$\Delta\Delta G = \Delta G_{\text{mut}} - \Delta G_{\text{HEL}}.$$

RESULTS

Hydrogen bonds at the antibody–antigen binding interface

S. Mohan and S. J. Smith-Gill (submitted) reported that, among the three antibodies, HH8Fv has the fewest and HH26Fv has the largest number of intermolecular hydrogen bonds and Van der Waals contacts in their respective complexes with HEL. Using different criteria (see Materials and Method) and the distance cut-offs (3.5 versus 3.0 Å) for H-Bond detection, we also find the same ranking among the three HH-HEL complexes for intra- and intermolecular hydrogen bonds (Table 1; Appendix). Among the three, only HH26-HEL complex contains an intermolecular main chain–main chain hydrogen bond, connecting Asp-92_L (The subscript represents chain ID throughout the text: H, heavy chain; L, light chain; Y, lysozyme.) to epitope residue Arg-21_Y (Fig. 2 *f*), implying close intermolecular associations. Epitope residue Arg-21_Y is a hot-spot of HH-HEL binding (Pons et al., 1999; Li et al., 2000, 2001), and, among the three antibodies, HH26 is most sensitive toward the mutations of this residue (Lavoie et al., 1999). Our results are consistent with previous reports that the interactions in antibody–antigen complexes are mainly via side chains, in contrast to interactions in proteinase–proteinase inhibitors, which are via main-chain atoms (Jackson, 1999). The ranking of the number of intra- and intermolecular hydrogen bonds (HH8 < HH10 < HH26) suggests that nonbonded interactions are least rigorous in HH8-HEL, most rigorous in HH26-HEL, and are intermediate in HH10-HEL.

TABLE 1 Hydrogen bonds at CDRs and Epitope

H-bond*	HH8-HEL			HH10-HEL			HH26-HEL		
Type	Intra	Inter	Total	Intra	Inter	Total	Intra	Inter	Total
MC-MC†	24	None	24	35	None	35	34	1	35
MC-SC‡	35	2	37	28	3	31	33	4	37
SC-SC§	2	1	3	3	2	5	3	3	6
Total	61	3	64	66	5	71	70	8	78

Summary of the number of hydrogen bonds present at the CDRs and epitope regions of HH8-HEL, HH10-HEL, and HH26-HEL complexes. Appendix provides the details.
*Hydrogen-bond.
†Main-chain–main-chain.
‡Main-chain–side-chain.
§Side-chain–side-chain.

Intramolecular salt bridges

Computational and experimental analysis have shown that salt bridges can be stabilizing (Marqusee and Sauer, 1994; Xu et al., 1997a; Lounnas and Wade, 1997) or destabilizing (Hendsch and Tidor, 1994; Sun et al., 1991). Thermophilic proteins have stronger salt bridges than their mesophilic counterparts (Yip et al., 1998; Kumar et al., 2000), indicating the functional significance of strong salt bridges. Electrostatic strength of salt bridges have been linked to protein flexibility (Sinha et al., 2001a,b). The three HH-HEL complexes were computed for the number and electrostatic strength of salt bridges. The electrostatic strengths of salt bridges were computed using the continuum electrostatic method described by Hendsch and Tidor (1994). This method, widely used to quantitatively estimate electrostatic potentials, pH-dependent properties, and solvation free energies (Honig and Nicholls, 1995), models proteins in atomic details and treats solvent as a bulk. The three components of salt-bridge strength (Hendsch and Tidor, 1994)

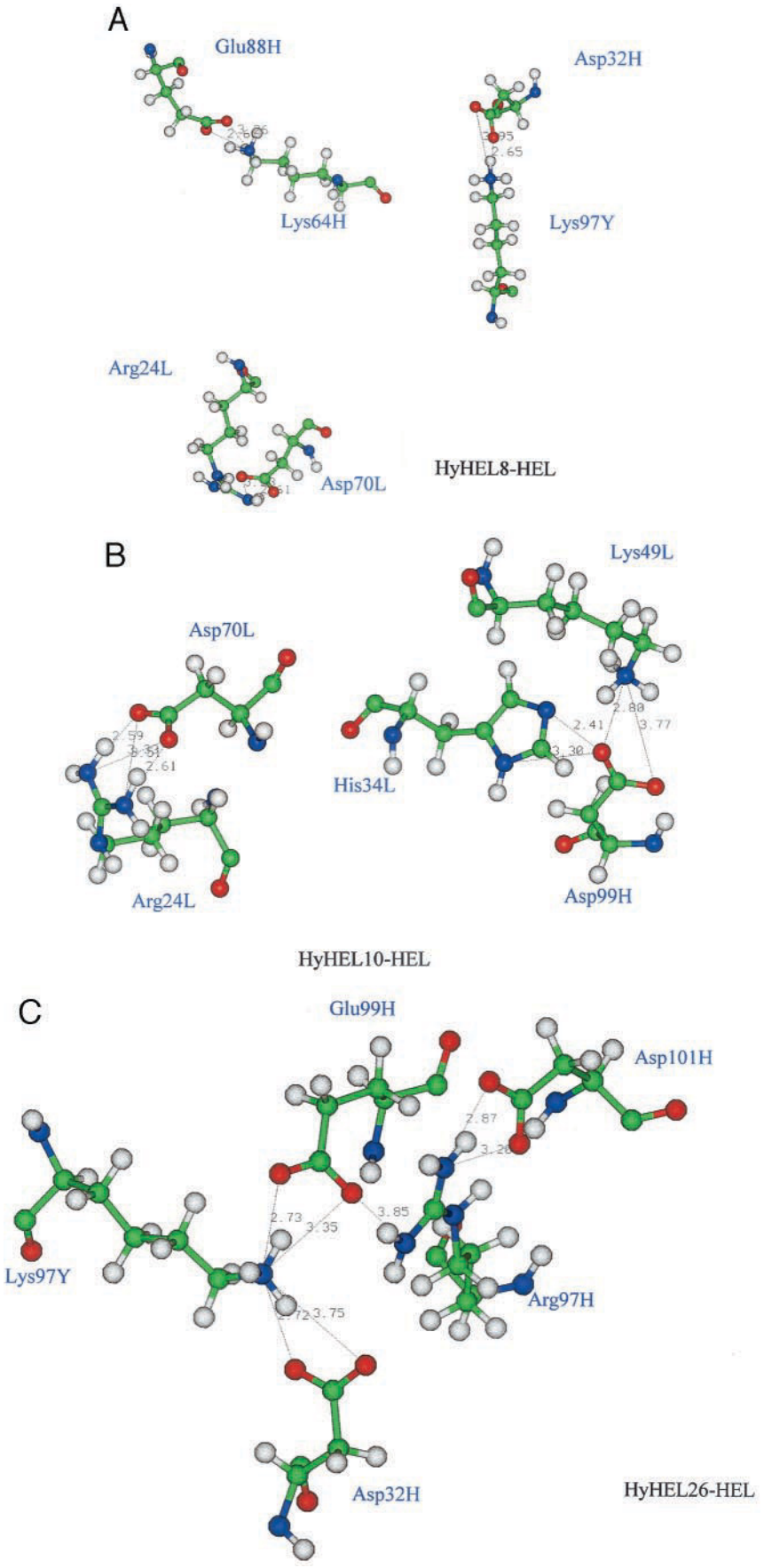

FIGURE 2 Salt bridges at the binding interface of HH8-HEL, HH10-HEL, and HH26-HEL complexes. (*a*) HH8-HEL: An intermolecular and two intramolecular salt bridges. (*b*) HH10-HEL: An intramolecular triad and an independent intramolecular salt-bridge. (*c*) Pentad present at the HH26-HEL binding interface. Intermolecular triad networked with intramolecular triad forms this pentad. The other two salt bridges present at the HH26-HEL interface (Table 2) are not shown in this picture. Salt bridges are shown as they map in the protein structure, whether networked or independent. Residues forming salt bridges are labeled: L, light chain; H, heavy chain; Y, HEL. Residue positions follow the chain names, which are followed by three-letter residue code. Distances between salt-bridge forming side-chains are shown in Å. (*d*, *e*, *f*) The complexity of salt-bridge interactions at the binding interfaces of (*d*) HH8-HEL, (*e*) HH10-HEL, and (*f*) HH26-HEL. Heavy chains are shown in purple, light-chains in yellow, and HEL in red. Salt-bridge-forming residues are shown in green and by their side chains. Residues forming an intermolecular (between light chain and HEL) main chain–main chain hydrogen bond, in the case of HH26-HEL, are shown in light blue and by their side chains. Picture is generated using Insight II package.

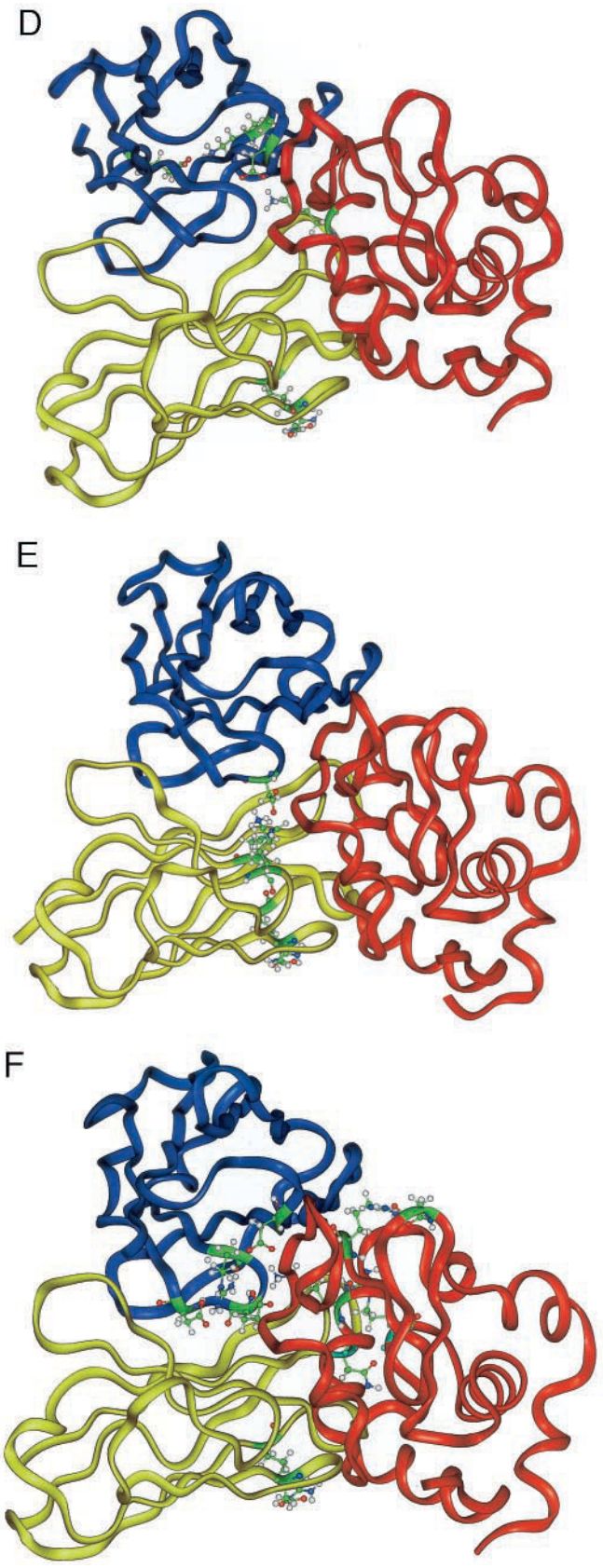

are salt-bridge interaction with solvent, electrostatic interaction between salt-bridging side chains, and salt-bridge interaction with the charges in the rest of the protein.

S. Mohan and S. J. Smith-Gill (submitted) reported that, among the three antibodies, the HH8-HEL complex had the fewest and HH26-HEL complex the largest number of intramolecular salt bridges in the Fv regions. They hypothesized that the differences in the number of intramolecular salt bridges account for differences in flexibilities and packing densities among the three Fvs. Using more stringent criteria for detecting salt bridges (see Materials and Methods) we also found that the HH8-HEL complex has fewer intramolecular salt bridges than either the HH10-HEL or HH26-HEL complexes (Table 2). In addition, the strengths of the intramolecular salt bridges at the binding site differ among the three complexes, being weakest in HH8-HEL and strongest in HH26-HEL (Table 3).

An intramolecular salt bridge, Lys-49_L—Asp-101_H was identified in HH10-HEL and HH26-HEL complexes by Mohan and Smith-Gill. This interaction did not qualify as a salt bridge according to our criteria (see Materials and Methods). We have computed the electrostatic strengths of this ion pair to estimate the qualitative differences in these complexes. This ion pair is very strong, −14.956 kcal/mol, in HH26-HEL and only marginally stabilizing, −0.106 kcal/mol, in HH10-HEL. The very high stability of this ion-pair in HH26-HEL is mainly due to the very favorable protein term of HH26-HEL.

Salt-bridge networks and electrostatic forces at the antibody–antigen interface

The numbers, electrostatic strengths, arrangement complexities, and the degree of networking of salt bridges at the binding interface vary among the three complexes (Table 3, Fig. 3). HH8-HEL has one intermolecular salt bridge, and HH26-HEL has two, which are networked. The single intermolecular salt bridge, Asp-32_H—Lys-97_Y, in HH8-HEL is only marginally stabilizing with an electrostatic strength less than −2.0 kcal/mol (Table 3). In contrast, this salt bridge contributes nearly −8.0 kcal/mol in HH26-HEL complex (Table 3). The second intermolecular salt bridge in HH26-HEL also involves Lys-97_Y, and contributes over −11.0 kcal/mol. The electrostatic contribution correlates well with alanine scanning data, which show that Lys-97_Y is a hot-spot residue (contributing −4.0 kcal/mol or more to the binding energy) in the epitopes of HH10, HH26, and the related antibody HH63 (Pons et al., 1999; Li et al., 2000), but contributes only slightly over −1 kcal/mol in the HH8 complex (see next section).

HH10-HEL was reported to contain the Asp-32_H—Lys-97_Y intermolecular salt bridge (Padlan et al., 1989), based on the criterion that their oppositely charged atoms were present within a 3.4-Å distance. This interaction does not meet the two criteria of our method (see Materials and Methods) to qualify as a salt bridge in HH10-HEL complex.

TABLE 2 Salt bridges in antibody variable domain–HEL complexes

Salt Bridge	Corresponding Regions	Complex			
		HH8-HEL	HH10-HEL	HH10Fv-HEL	HH26-HEL
Inter-molecular					
$Asp\text{-}32_H$–$Lys\text{-}97_Y$	CDR1-Epitope	✓	–	✓	✓
$Glu\text{-}99_H$–$Lys\text{-}97_Y$	CDR3-Epitope	–	–	–	✓
Intra-molecular					
$Lys\text{-}64_H$–$Glu\text{-}88_H$	CDR2-Frame (B)*	✓	–	–	–
$Arg\text{-}66_H$–$Asp\text{-}89_H$	Frame	✓	✓	✓	✓
$Arg\text{-}24_L$–$Asp\text{-}70_L$	CDR1-Frame (B)	✓	✓	–	✓
$Arg\text{-}61_L$–$Glu\text{-}79_L$	Frame	✓	✓	✓	–
$Arg\text{-}61_L$–$Asp\text{-}82_L$	Frame	✓	✓	✓	✓
$Arg\text{-}38_H$–$Glu\text{-}46_H$	Frame	–	✓	–	–
$Asp\text{-}99_H$–$His\text{-}34_L$	CDR3-CDR1 (B)	–	✓	–	–
$Asp\text{-}99_H$–$Lys\text{-}49_L$	CDR3-CDR2 (B)	–	✓	–	–
$Lys\text{-}39_L$–$Glu\text{-}42_L$	Frame	–	✓	–	–
$Lys\text{-}39_L$–$Glu\text{-}81_L$	Frame	–	✓	–	–
$Lys\text{-}103_L$–$Glu\text{-}105_L$	Frame	–	✓	–	–
$Lys\text{-}1_Y$–$Glu\text{-}7_Y$	HEL	–	✓	✓	–
$Asp\text{-}119_Y$–$Arg\text{-}125_Y$	HEL	–	✓	–	✓
$Asp\text{-}72_H$–$Lys\text{-}75_H$	Frame	–	–	✓	–
$Asp\text{-}48_Y$–$Arg\text{-}61_Y$	HEL (B)	–	–	✓	✓
$Arg\text{-}97_H$–$Glu\text{-}99_H$	Frame-CDR3 (B)	–	–	–	✓
$Arg\text{-}97_H$–$Asp\text{-}101_H$	Frame-CDR3 (B)	–	–	–	✓
$Glu\text{-}42_L$–$Arg\text{-}45_L$	Frame	–	–	–	✓
$Asp\text{-}66_Y$–$Arg\text{-}68_Y$	HEL	–	–	–	✓

Salt bridge-forming residues are shown by their names, followed by the residue positions, followed by chain identifications. Criteria for salt-bridge detection is as described in text.

*Binding site; only shown in cases of intramolecular salt bridges.

First, the Oδ1 atom of aspartate was not within the 3.4-Å distance from Nζ atom of lysine; the distance was found to be 3.6 Å. Second, although the distance was within 4 Å, a limit set in our method, the distance between the centroid of their opposite-charged groups were more than 4.0 Å. However, there is still an electrostatic interaction between these

TABLE 3 Electrostatic contributions of salt bridges present at the binding site

Complex	Salt Bridge*	$\Delta G_{desolve}$ (kcal/mol)	ΔG_{bridge} (kcal/mol)	$\Delta G_{protein}$ (kcal/mol)	Total (ΔG_{elect}) (kcal/mol)
Intermolecular salt bridges (between antibody and hen egg white lysozyme)					
HH8-HEL	$Asp\text{-}32_H$–$Lys\text{-}97_Y$	10.89	−8.25	−4.64	−2.00
HH10Fv-HEL	$Asp\text{-}32_H$–$Lys\text{-}97_Y$	19.02	−13.37	−18.72	−13.07
HH26-HEL	$Asp\text{-}32_H$–$Lys\text{-}97_Y$	17.36	−11.46	−13.68	−7.78
HH26-HEL	$Glu\text{-}99_H$–$Lys\text{-}97_Y$	16.37	−11.80	−16.05	−11.48
Intramolecular salt bridges (binding region)					
HH8-HEL	$Lys\text{-}64_H$–$Glu\text{-}88_H$	8.73	−6.43	−3.05	−0.75
HH8-HEL	$Arg\text{-}24_L$–$Asp\text{-}70_L$	0.80	−1.70	−0.38	−1.28
HH10-HEL	$Asp\text{-}99_H$–$His\text{-}34_L$	15.06	−5.91	−8.09	1.06
HH10-HEL	$Asp\text{-}99_H$–$Lys\text{-}49_L$	18.89	−11.50	−13.79	−6.40
HH10-HEL	$Arg\text{-}24_L$–$Asp\text{-}70_L$	1.22	−1.89	−0.12	−0.79
HH10Fv-HEL	$Arg\text{-}66_H$–$Asp\text{-}89_H$	12.68	−7.35	−10.93	−5.60
HH10Fv-HEL	$Asp\text{-}48_Y$–$Arg\text{-}61_Y$	10.09	−1.66	−8.43	−0.01
HH26-HEL	$Arg\text{-}97_H$–$Glu\text{-}99_H$	12.92	−4.74	−20.44	−12.26
HH26-HEL	$Arg\text{-}97_H$–$Asp\text{-}101_H$	11.49	−12.54	−12.60	−13.65
HH26-HEL	$Arg\text{-}24_L$–$Asp\text{-}70_L$	1.24	−1.80	−0.23	−0.79
HH26-HEL	$Asp\text{-}48_Y$–$Arg\text{-}61_Y$	6.15	−4.71	−5.82	−4.38

The electrostatic contributions for intermolecular salt bridges and for those that are present at the binding site to the free energy of folding, calculated using continuum electrostatic approach, using finite difference methods to solve Poisson–Boltzmann equation, using DELPHI computer program developed by Honig and co-workers (Gilson et al., 1985; Gilson and Honig, 1987). If a salt bridge involves at least one residue either from epitope or from any of the CDRs, it is considered to be present at the binding site.

*Salt bridge-forming residues are shown. Residue names are followed by their positions, which are followed by chain identifications.

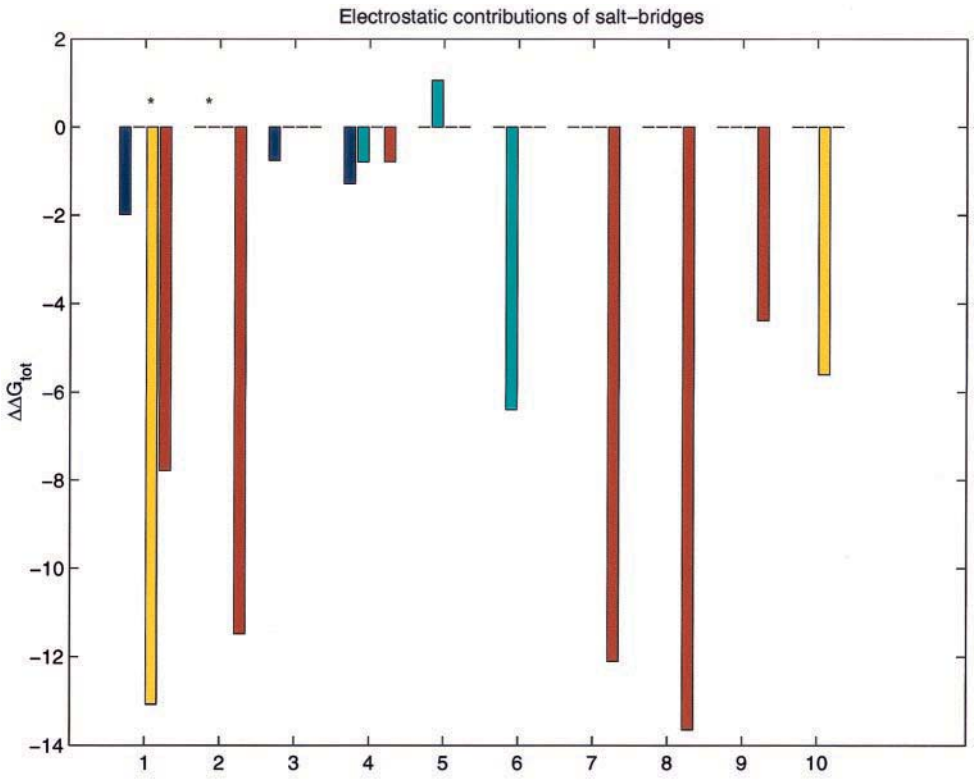

FIGURE 3 Plot showing the electrostatic strengths of the salt bridges present at the HH8-HEL (*blue*), HH10-HEL (*cyan*), HH10Fv-HEL (*yellow*), and HH26-HEL (*red*) binding interfaces. Electrostatic strength of salt bridges (ΔG_{tot}) is shown in kcal/mol. The numbers on the *x* axis represents the following salt bridges: 1, D32H-K97Y; 2, E99H-K97Y; 3, K64H-E88H; 4, R24L-D70L; 5, D99H-H34L; 6, D99H-K49L; 7, R97H-E99H; 8, R97H-D101H; 9, D48Y-R61Y; 10, R66H-D89H (first character is one-letter residue code, followed by residue position, which is followed by the chain identification). *, Intermolecular salt bridge.

two residues, forming an ion pair, but its electrostatic strength is insignificant (0.07 kcal/mol).

The recently solved crystal structure of HH10Fv domain complexed with HEL, at 1.8-Å resolution (Kondoi et al., 1999) shows that the intermolecular salt bridge, Asp-32_H–Lys-97_Y, not present in HH10Fab-HEL, is present in HH10Fv-HEL (Table 2). In addition, HH10Fv-HEL buries a larger proportion of surface area and has more favorable interactions than the HH10Fab-HEL complex (Kondoi et al., 1999), and has minor conformational differences from HH10Fab-HEL at the binding interface (Kondoi et al., 1999). Analysis of intramolecular salt bridges shows that the HH10Fv-HEL complex also has fewer intramolecular salt bridges within the Fv than either of the three Fab-HEL complexes, and includes one between framework residues that is unique to that complex (Tables 2 and 3). Because the affinity of the HH10Fv-HEL complex is significantly lower than that of the HH10Fab-HEL complex (Kondoi et al., 1999), it may not be a representative of the molecular interactions of either HH10-Fab or HH10-Ig with HEL, even though the structure is of higher resolution. It has been suggested that the unfavorable effect of removing the constant region was compensated by favorable interactions between HH10 and HEL, in the case of HH10Fv-HEL complex (Kondoi et al., 1999). Nonetheless, the presence of the intermolecular salt bridge in the HH10Fv-HEL complex indicates an electrostatic interaction between these two residues. In addition, our Ala scanning data (next section) indicates that Lys-97_Y contributes ≥ -4.0 kcal/mol to binding, and HH10Fab-HEL double-mutant cycle analysis suggests a significant energetic interaction between Lys-97_Y and Asp-32_H (Pons et al., 1999).

In HH8-HEL, there are no salt-bridge networks, and the electrostatic strengths of the binding site salt bridges are very low (Table 3). In HH10-HEL, the two CDR inter-chain salt bridges are networked to form a triad, with relatively high electrostatic contributions. One of the salt bridges of the intramolecular triad is significantly stabilizing, and the other is marginally destabilizing. The total electrostatic strength of the triad is significantly high (Table 4).

Two intramolecular salt bridges in HH26-HEL form a triad, and are further networked with an intermolecular triad to form a pentad (Fig. 2 *c*). All salt bridges of this network are strongly stabilizing (-7.78 kcal/mol or more), suggesting a functional/structural significance of the pentad. The total electrostatic strength of the pentad is very high (Table 4), as expected, because all four salt bridges within this network are strongly stabilizing (Table 3). Table 4 summarizes the components of the pentad electrostatic strength, and their electrostatic contributions. The pentad is considered as a unit, and its electrostatic strength is computed as described for salt bridges (see Materials and Methods). We have computed the bridge terms for all possible electrostatic interactions present in the pentad (Table 4). It is clear from Table 4 that destabilization due to unfavorable interactions between like charges is much smaller than the stabilization due to the favorable interactions between opposite charges. In the case of the triad, present in HH10-HEL, the

TABLE 4 Electrostatic contribution of Triad in HH10-HEL and Pentad in HH26-HEL

Triad		
Desolvation penalty (Kcal/M)		
Residue side chain	Penalty	Total
Asp-99_H	8.82	
His-34_L	3.37	
Lys-49_L	8.04	20.23
Bridge terms (Kcal/M)		
Interaction type	Bridge term	Total
Asp-99_H–Lys-49_L	−11.50	
Asp-99_H–His-34_L	−5.91	
Lys-49_L–His-34_L	6.65	−10.76
Protein term (Kcal/M)		
Interaction	Protein term	
Triad–rest of the protein	−15.75	−15.75
Total electrostatic strength of Triad (Kcal/M)		−6.28
Pentad		
Desolvation penalty (Kcal/M)		
Residue side chain	Penalty	Total
Asp-32_H	5.94	
Lys-97_Y	7.64	
Glu-99_H	4.84	
Arg-97_H	2.58	
Asp-101_H	4.80	25.80
Bridge term (Kcal/M)		
Interaction type	Bridge term	Total
Asp-32_H–Lys-97_Y	−11.49	
Asp-32_H–Glu-99_H	+4.00	
Asp-32_H–Arg-97_H	−3.57	
Asp-32_H–Asp-101_H	+1.27	
Lys-97_Y–Glu-99_H	−11.89	
Lys-97_Y–Arg-97_H	+2.92	
Lys-97_Y–Asp-101_H	−1.54	
Glu-99_H–Arg-97_H	−4.80	
Glu-99_H–Asp-101_H	+3.43	
Arg-97_H–Asp-101_H	−12.59	−34.26
Protein term (Kcal/M)		
Interaction	Protein term	
Pentad–rest of the protein	−24.86	−24.86
Total electrostatic strength of Pentad (Kcal/M)		−33.32

Electrostatic contribution of salt-bridge networks in HH10-HEL and HH26-HEL complexes. Charge desolvation penalty is computed for all the side chains. All possible electrostatic interactions in the network were computed for their potentials. Method is detailed in Materials and Methods section. Residue names are followed by their positions, which is followed by chain identifications.

destabilization due to unfavorable interaction is also high (Table 4). Electrostatic interaction of the pentad with the rest of the protein is also very favorable (Table 4). The strong electrostatic strength further corroborates the functional value of pentad, and the constituent salt bridges. It is possible that this pentad is acquired during the affinity maturation of the HH26 antibody, and is a major determinant of the high HH26-HEL binding specificity.

Only the HH26-HEL complex has an intramolecular salt bridge, Asp-48_Y–Arg-61_Y (also present in HH10Fv-HEL). This ion pair is also present in uncomplexed HEL. (Table 3, Fig. 3), in the epitope region of HEL, which is significantly stabilizing. In HH10Fv-HEL, the intermolecular salt bridge, Asp-32_H–Lys-97_Y is significantly stabilizing, but is not networked. One intramolecular salt bridge is stabilizing, but the other intramolecular salt bridge, Asp-48_Y–Arg-61_Y, present at the HEL binding site, is almost neutral.

The desolvation penalties, the bridge terms and the protein terms of the salt-bridge formation vary among the three complexes. Salt bridges in HH8-HEL pay lower desolvation penalties than salt bridges in HH10-HEL and HH26-HEL complexes. HH26-HEL salt bridges pay the highest desolvation penalties. Yet, this heavy penalty in HH26-HEL is compensated by very favorable bridge and protein terms. In HH10-HEL, on average, bridge and protein terms are more favorable than the HH8-HEL and less favorable than HH26-HEL. The bridge and protein terms in HH8-HEL salt bridges are only moderately favorable. The more a salt bridge is buried, the higher desolvation penalty it pays, but it will have stronger electrostatic interactions due to absence of solvent screening. The extent of the electrostatic protein environment will further determine the robustness of the charge–charge interactions between the salt-bridging side chains.

The higher number of salt bridges, the networking of very strong salt bridges, the preservation of the intramolecular salt bridge at the binding site of HEL, which is absent in HH8-HEL and HH10-HEL complexes, indicate an inherently electrostatic binding of HH26-HEL, which is likely to be a significant factor for high binding specificity of HH26 toward HEL. In contrast, weak electrostatic interactions may predispose HH8-HEL binding to be less specific. The weak electrostatic component of HH8-HEL binding implies an inherent flexible nature of the HH8-HEL binding site.

Electrostatic and hydrophobic components of binding

Conformationally flexible parts have relatively lower electrostatic interactions, and substantial hydrophobic interactions (Sinha et al., 2001a,b). We have examined the total electrostatic and hydrophobic contributions to the free energy of HH8, HH10, and HH26 binding to HEL (Table 5). Both antigen and antibody pay heavy charge desolvation penalties upon binding in all three complexes, but there are large differences among the three complexes in the electrostatic components of binding. HH10-HEL has significantly favorable electrostatic component in comparison to HH8-HEL, but it is less favorable in comparison to HH26-HEL. HH10-HEL and HH26-HEL are more similar to each other than to HH8-HEL. Their desolvation penalties are higher than that of HH8 by 4–5 kcal/mol, and they differ from each other by only 1 kcal/mol. HH10 and HH26 have −7.0 to −10.0 kcal/mol more favorable electrostatic interactions with HEL than HH8 with HEL, with a difference between them of −3.0 kcal/mol. Overall, the electrostatic contribution to the free energy of binding is lowest in HH8-HEL, intermediate in HH10-HEL, and highest in HH26-HEL. Among the three complexes, HH8-HEL has largest hydrophobic contributions. Compared to the differences in

TABLE 5 Binding free energies and their electrostatic and hydrophobic components

Complex		Experimental (SPR)		Desolvation					
Antigen	Antibody	ΔG	$\Delta\Delta G_{m-w}$	Antibody	HEL	Total	ΔG_{el}	ΔG_{hydro}	$\Delta\Delta G_{m(e+h)-w(e+h)}$
HEL	HH8	−13.8		24.24	25.84	50.08	−13.31	−47.95	
	HH10	−13.1		24.28	31.68	55.96	−20.66	−44.05	
	HH26	−10.4		28.19	26.51	54.70	−23.88	−46.16	
HEL(K96A)	HH8	−13.1	0.7	21.63	20.94	42.57	−7.15	−47.62	−1.02
	HH10	−12.8	0.3	23.05	23.44	46.49	−13.33	−44.03	−2.12
	HH26	−10.8	−0.3	26.34	24.26	50.60	−13.90	−45.92	6.12
HEL(K97A)	HH8	−12.300	1.4	21.52	23.20	44.72	−5.50	−48.17	2.23
	HH10	−9.000	4.1	24.24	23.80	48.04	−6.10	−43.99	6.70
	HH26	−6.800	3.6	26.11	22.29	48.40	−2.91	−47.35	13.48

Binding free energies and their components are in kcal/mol. $\Delta\Delta G_{m(e+h)-w(e+h)}$ is calculated only taking into account the electrostatic and hydrophobic components. Our purpose is to have a qualitative estimate of the effects of Lys-97_Y and Lys-96_Y mutants on the three HH-HEL complexes. Our calculations correspond qualitatively to experimental observations that the Lys-97_YAla mutants affect the binding more severely than Lys-96_YAla mutant.
ΔG_{desol} is the charge desolvation penalty.
ΔG_{el} is the electrostatic energy between antibody and antigen (equivalent to the bridge term in salt bridge free energy calculations).
ΔG_{hydro} is the hydrophobic component of the free energy of binding.
The calculations were performed as described in the text.

electrostatic contributions, the hydrophobic contributions are similar among all the complexes and their mutants. Significant differences are in electrostatic contributions. The finding is consistent with the earlier result that HH26 is more electrostatic in nature. We hypothesize that higher electrostatics make HH26 binding site more rigid and less cross-reactive.

Binding of HH8, HH10, and HH26 to Lys-97ala and Lys-96ala mutants of HEL

Previous alanine scanning mutagenesis showed that only three hot-spot epitope residues contribute more then 4 kcal/mol to the free energy of HH10-HEL complex formation (Pons et al., 1999). These three residues were reported to be Lys-97_Y, Lys-96_Y and Tyr-20_Y, where Lys-96_Y contributed the most, based on enzymatic activity assay (Pons et al., 1999). We modeled alanine mutants of the two charged epitope residues, Lys-96_Y and Lys-97_Y and calculated their electrostatic and hydrophobic components of binding. The impacts of these mutations on binding kinetics were also measured by SPR using site-directed mutants of HEL(K96A) and HEL(K97A). These two sequentially adjacent charged residues were particularly selected because, although adjacent residues on HEL, only Lys-97_Y forms an intermolecular salt-bridge, and because these two residues have been shown experimentally to be the hot-spots of binding (Pons et al., 1999). The analysis of the charged hot-spot mutants would allow straightforward estimation of the qualitative differences in the electrostatic properties of the three complexes.

SPR results confirm previous findings that Lys-97_Y is a hot spot residue in all three complexes, but showed that the energetic contribution of Lys-96_Y to binding is insignificant (Table 5). In fact, SPR studies show that, among all the epitope residues, Lys-97_Y contributes the largest amount to the free energy of binding in HH10-HEL and HH26-HEL complexes (S. J. Smith-Gill, C. A. Lipschultz, Y. Li, and S. Mohan, unpublished results). For HEL(K97A) complexes, $\Delta\Delta G$ ranked HH8 < HH10 < HH26 (Table 5). For all three antibodies, the greatest impact of Lys-97_Y mutations on free energy change is at the encounter step of association (Fig. 4), which is consistent with the view that electrostatic forces play an important role in steering and orienting the molecules to form the encounter complex (Sines et al., 1990; Kozack et al., 1995; Antosiewicz and McCammon, 1995; Janin, 1997). The impact of HEL(K97A) mutation on free energy change of HH8 docking is insignificant ($\Delta\Delta G2 <$ 0.5 kcal/mol). Experiments based on a lysozyme enzymatic activity assay (Pons et al., 1999) reported Lys-97_Y to contribute less then Lys-96_Y. The discrepancy may be due to the different buffer and pH conditions used, which may affect the protonation states of the charged groups. In an earlier study, it has been shown that the binding of HH10 to HEL with the mutants of charged epitope hot-spot residues is significantly pH dependent, where the shifts in pKas due to mutations would result in proton uptake or release (Sharp, 1998). Additionally, SPR results are directly calculated from binding data (at pH 7.4), whereas the results of Pons et al. (1999) are derived indirectly by estimating free lysozyme via enzymatic activity, at pH 6.0.

Examination of the individual rate constants (Fig. 5, *a–c*) shows that the mechanisms underlying the encounter thermodynamic changes differ among the antibodies. For the HH8-HEL(K97A) complex, the association and dissociation rate constants of the encounter step (k_{+1} and k_{-1}), are slowed and increased by 2–2.5 fold, respectively (Fig. 5 *a*), resulting in a net loss of ~−1.0 kcal/mol from the encounter step (Fig. 4 *a*). The lower k_{+1} reflects a small increase of ~0.5 kcal/mol in activation energy for encounter (Fig. 4 *b*), whereas loss of ~1 kcal/mol from $\Delta G1$ and slightly higher

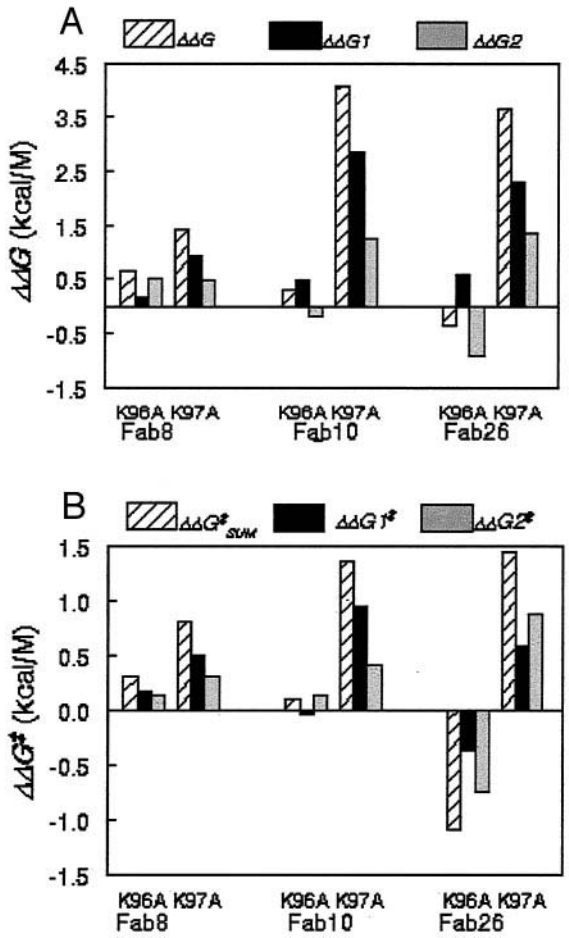

FIGURE 4 The binding kinetics of these mAbs conformed well to a two-step kinetic model describing an "induced fit" binding mode

$$\mathrm{A} + \mathrm{B} \underset{k_{-1}}{\overset{k_{+1}}{\leftrightharpoons}} [\mathrm{AB}] \underset{k_{-2}}{\overset{k_{+2}}{\leftrightharpoons}} \mathrm{AB}.$$

To obtain estimates of the rate constants, a data set containing association times (T_a) of at least two durations (Lipschultz et al., 2000) was analyzed globally to obtain estimates of rate constants. The parameters k_{+1}, k_{-1}, k_{+2}, k_{-2}, and R_{max} were estimated with BIAeval 3.0.2 software (Biacore, Inc., Uppsala, Sweden), which uses the Marquat–Levenberg algorithm to simultaneously iteratively fit binding data of all curves within a given data set (global fit) to simultaneous rate equations,

$$\frac{\mathrm{dB}}{\mathrm{d}t} = k_{-1}\cdot[\mathrm{AB}]^* - k_{+1}\cdot\mathrm{A}\cdot\mathrm{B},$$

$$\frac{\mathrm{d}[\mathrm{AB}]^*}{\mathrm{d}t} = (k_{+1}\cdot\mathrm{A}\cdot\mathrm{B} - k_{-1}\cdot[\mathrm{AB}]^*) - (k_{+2}\cdot[\mathrm{AB}]^* - k_{-2}\cdot\mathrm{AB}),$$

$$\frac{\mathrm{dAB}}{\mathrm{d}t} = k_{+2}\cdot[\mathrm{AB}]^* - k_{-2}\cdot\mathrm{AB},$$

where $B(0) = R_{max}$, $[AB]^*(0) = AB(0) = 0$, and total $RU = [AB]^* + AB$. Error terms were all less than 5% of the mean. Calculations were performed carrying three significant figures. Equilibrium constants were calculated from the mean rate constants (Krauss et al., 1976; Barre et al., 1994; Lipschultz et al., 2000).

k_{-1} suggests that encounter complex is also less stable than that of HEL complex. This is reflected in the higher T_{50}, which is a measure of the biological half-life of conversion of encounter complex to docked complex (Fig. 6, *a* and *d*). The apparently faster net off-rate (Fig. 5 *d*) reflects a higher proportion of complexes in the less stable encounter state (Fig. 6 *d*).

In contrast to the HH8-HEL(K97A) complex, although the encounter association rate constants (k_{+1}) of the HH10-HEL(K97A) and HH26-HEL(K97A) complexes are slowed by about the same order of magnitude as that of HH8-HEL(K97A) (~5× and 2.5×, respectively), the encounter dissociation constants (k_{-1}) of both complexes are increased by about 20-fold (~25× and 18×, respectively) (Fig. 5, *b* and *c*). In both the HH10-HEL and HH26-HEL complexes, the loss of Lys-97 destabilizes the encounter complex (Fig. 5, *b* and *c*) and increases the activation energy required for encounter (Fig. 4 *b*). The loss of the electrostatic interaction with Lys-97_Y increases the encounter activation energy of HH10-HEL more than that of HH26-HEL complex, and increases the docking activation energy of HH26-HEL more than that of HH10-HEL complex (Fig. 4 *b*). The effects on the rate constants for the docking step are less dramatic, with 2–4-fold decrease in k_{+2} and a 2–4-fold increase in k_{-2} (Fig. 5, *b* and *c*). In both complexes, the large increase in k_{-2}, coupled with smaller decrease in k_{+2}, results in $k_{+2} < k_{-1}$, and the rate-limiting step is shifted from the encounter to docking, consistent with the increase in the activation energy for docking in

$$K_{a1} = \frac{k_{+1}}{k_{-1}}; \quad K_{a2} = \frac{k_{+2}}{k_{-2}}; \quad \text{and} \quad K_A = K_{a1}(1 + K_{a2}).$$

(*a*) Free energy changes were calculated from the equilibrium constants (Lipschultz et al., 2000; Li et al., 2001)

$$\Delta G1 = -RT\ln(K_{a1})$$

$$\Delta G2 = -RT\ln(K_{a2}),$$

$$\Delta G^\circ = \Delta G1 + \Delta G2.$$

In all cases, total ΔG calculated as above did not differ from ΔG calculated directly from overall equilibrium constant K_A. (*b*) The activation energies for the encounter and docking stages ($\Delta G1^{\ddagger}$ and $\Delta G2^{\ddagger}$) were calculated from k_{+1} and k_{+2}, respectively (S. Mohan et al., submitted), where, according to the transition state theory,

$$\Delta G^{\ddagger} = -RT\,\mathrm{in}(K^{\ddagger}),$$

$$\Delta\Delta G^{\ddagger} = -RT\,\mathrm{in}(K^{\ddagger}_{mut}/K^{\ddagger}_{HEL}),$$

where $K^{\ddagger} = k_B T k_a/\hbar$, k_a is the forward rate constant, k_B is Boltzmanns constant and $\hbar$ is Planck's constant.

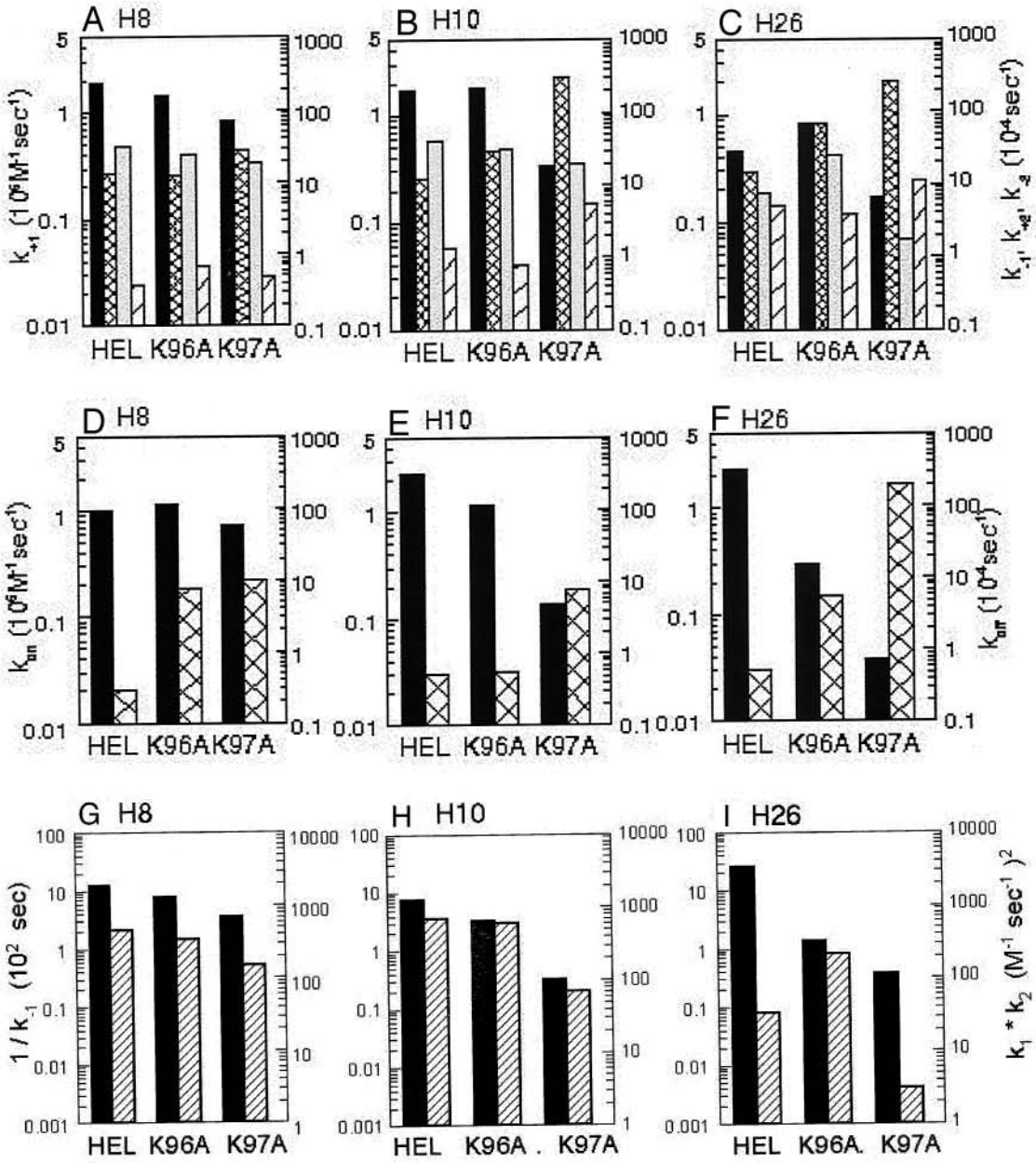

FIGURE 5 (*a–c*) Rate constants for two-step association of (*a*) HH8, (*b*) HH10, and (*c*) HH26 complexes with HEL, HEL(K96A) and HEL(K97A), calculated as described in Fig. 4. *Solid black*, k_{+1}; *cross-hatched*, k_{-1}; *gray*, k_{+2}; *diagonal*, k_{-2}. k_{+1} is plotted on left axis; k_{-1}, k_{+2}, k_{-2} on the right axis. (*d–f*) Apparent association and dissociation rate constants of (*d*) HH8, (*e*) HH10, and (*f*) HH26 complexes with HEL, HEL(K96A), and HEL(K97A) were estimated from same data as (*a–c*) with BIAeval 3.0.2 software (Biacore Inc.), using Langmuir model. *Solid black*, k_{on} (left axis); *cross-hatch*, k_{off} (right axis). (*g–i*) Relative stability of the encounter complex are represented as $1/k_{-1}$ (*Solid black, left axis*), and relative strengths of the close range steering effects (*cross-hatch, right axis*) as the product of the forward rate constants, $k_{+1}k_{+2}$ (Selzer and Schreiber, 2001).

both complexes (Fig. 4 *b*). Thus, a smaller proportion of the complexes actually dock, and stabilities of the docked mutant complexes are lower than the stabilities of docked HEL complexes (Fig. 5, *h* and *i* and Fig. 6, *e* and *f*). The relative overall impact of the mutations on steering is related to the product k_1k_2, whereas the stability of encounter complex is proportional to $1/k_{-1}$ (Selzer and Schreiber, 2001). The mutation K97A affects the stability and the steering by about the same order of magnitude for each of the HH8-HEL and HH10-HEL complexes.

Because of the impact of slower docking and a faster dissociation of the encounter complexes, the impact of the mutations on the apparent association and dissociation rates are exaggerated (Fig. 5, *d–f* and Fig. 6, *j–l*). The apparent association appears to be much slower than it is because docking has become rate limiting. This can be seen in the

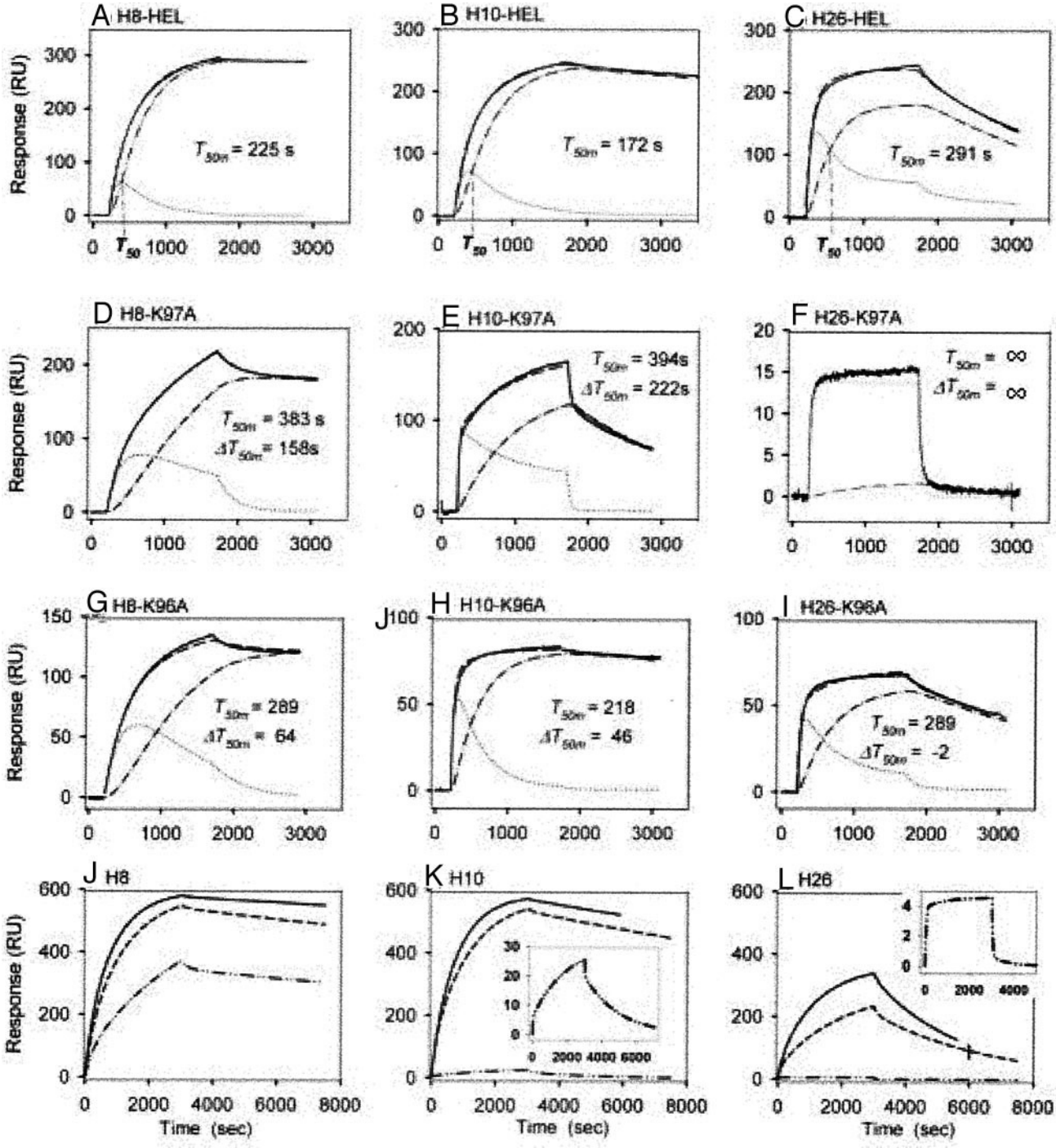

FIGURE 6 (*a–i*) Representative sensograms of binding of the three Fabs to HEL and mutant antigens. The rate constants (k_{+1}, k_{-1}, k_{+2}, k_{-2}), calculated as described in the legend to Fig. 4 and shown in Fig. 5, were used to simulate the component curves for the encounter complex, [AB]*, and the docked complex, AB. In each panel ——, the original binding data; ····, [AB]*; ···-··-, AB; and - - -, the fitted total binding. We define the point at which the [AB]* and AB curves cross as T_{50}, where [AB]* = AB = 50% (RU_{total}) (illustrated on time axis of panels *a–c*). Values for T_{50}, determined from simulations at 10-nM concentrations and a series of increasing concentrations until T_{50} asymptotes at a minimum value ($T_{50}m$), using the rate constants determined by global analysis (Figs. 4 and 5). $T_{50}m$ is a parameter that is unique and characteristic of each complex. When k_{+1} is rate limiting (i.e., $k_{-2} < k_{+2}$) $T_{50}m = t½$ of k_{+2} (Lipschultz et al., 2000). All values are given in seconds. The values for $\Delta T_{50}m$ were calculated as $T_{50}m_{mut} - T_{50}m_{HEL}$ for each respective antibody. The Fab concentrations in the binding curves depicted are: (*a*, *d*, *g*) HH8 21 nM on all three antigens; (*b*) HH10 21 nM on HEL; (*c*) HH26 21 nM on HEL; (*e*) HH10 640 nM on HEL(K97A); (*f*) HH26 146 nM on HEL(K97A); (*h*) HH10 100 nM on HEL(K96A); (*i*) HH26 210 nM on HEL(K96A). (*j–l*) simulations of (*j*) HH8, (*k*) HH10, and (*l*) HH26 binding to HEL (——), HEL(K96A) (- - - -), and HEL(K97A) (– · · –). All antibodies are at a concentration of 10 nM. Insets show enlargements of HH10 and HH26 binding to HEL(K97A). Simulations are depicted to allow comparison of all complexes at the same concentration, which could not be reliably obtained experimentally because of the widely differing affinities.

association kinetics: an initial rapid association is followed by a slower prolonged association phase (Fig. 6, *e* and *f*), which results in a significantly slower net on rate using a 1-step Langmuir association model (Fig. 5, *e* and *f*). This is particularly true for the complexes of HH10 and HH26 with HEL(K97A). The encounter association rate constant k_{+1} in HH10-HEL(K97A) complex is ~5-fold lower (Fig. 5 *b*), but the apparent k_{on} is nearly 20-fold lower than the HH10-HEL complex (Figs. 5 *e* and 6 *k*). For the HH26-HEL(K97A) complex, the k_{+1} is ~3-fold lower (Fig. 5 *c*), whereas the apparent K_{on} is 60-fold lower than the HH26-HEL complex (Figs. 5 *f* and 6 *l*). For these complexes, the apparently large impact of the mutation on electrostatic steering is a combination of a decreased stability of the encounter complex and a slower conversion to the docked state. This can be clearly seen by comparing the simulated component curves of the respective HEL and HEL(K97A) complexes (Fig. 6, *a–f*). In the HH26-HEL(K97A) complex, docking is so severely affected that the majority of complexes never dock but rapidly dissociate. The HEL(K97A) mutation affects the transition states of the HH8 and HH10 encounter steps more than those of docking, but it affects the transition state of HH26 docking more than that of encounter.

The decreases in the free energy attributable to the Lys-96_Y substitution ($\Delta\Delta G_{mut\text{-}wild}$) are less than half a kcal/mol, and insignificant compared to Lys-97_Y (Figs. 4 and 5 *d–f*). For the complexes with HEL(K96A), the differences of Lys-96_Y contributions in the three complexes can again be attributed to the electrostatic nature of binding in HH26-HEL, where lysine, being a charged epitope residue, has a more important role in HH26-HEL binding than in HH8-HEL and HH10-HEL (Table 5). Calculations show that the net effect of Lys-96_Y on these two complexes is destabilizing, as indicated by favorable $\Delta\Delta G_{m(el+hydro)-w(el+hydro)}$, which is marginally negative in cases of HH8-HEL and HH10-HEL, showing that Lys-96_Y, by itself, does not contribute to the free energy of binding in these complexes. The computational data is supported by the experimental data (Table 5, Fig. 4). However, for both the HH10-HEL and HH26-HEL complexes, although the net $\Delta\Delta G$ is insignificant, $\Delta\Delta G1$ is ~0.5 kcal/mol, and, in HH26-HEL $\Delta\Delta G2$, is nearly −1.0 kcal/mol (Fig. 4). The $K97_Y$ mutation lowers the activation energy for HH26 docking by ~1 kcal/mol. The net impact of the mutation is unfavorable for both steps, but then stabilizing to the final complex in the case of HH26, as reflected by lower values of k_{-2}, and a higher k_{+2} for HH26.

Lys-97_Y forms an intermolecular salt bridge in HH8-HEL and HH26-HEL complexes. In the complexes with HEL(K97A), $\Delta\Delta G_{m(el+hydro)-w(el+hydro)}$ is largest for HH26, and smallest for HH8. The decrease in the free energy of binding in all three cases is due to the significant loss in the electrostatic contribution (Table 5). The loss is largest in HH26-HEL(K97A) and smallest in HH8-HEL(K97A), as compared to their respective wild types. Higher sensitivity of HH26 binding to HEL(K97A), as compared to HH8 and HH10, corresponds to the observation that the intermolecular salt bridge, formed between Lys-97_Y and Asp-32_H, is very strong in HH26-HEL and is only marginally stabilizing in HH8-HEL. The stabilizing impact of this electrostatic interaction is primarily on the encounter complex, with a smaller impact on post-encounter docking step. In the case of the HH10-HEL complex, although the interaction between Asp-32_H and Lys-97_Y did not qualify as a salt bridge, discussed above, the contribution of Lys-97_Y toward the free energy of binding was higher than in HH8-HEL complex, apparently due to the higher electrostatic nature of binding in HH10-HEL as compared to HH8-HEL.

The large impact on the encounter step of the HH10 complex is in contrast with the effect of other Ala mutants, which generally have a larger impact on docking than on encounter of this antibody (Li et al., 2001; S. J. Smith-Gill, C. A. Lipschultz, and Y. Li, unpublished data). The Lys-97_Y mutation has a slightly greater effect on docking of HH26 than on HH10.

Considering that Lys-97_Y forms a stable intermolecular salt bridge, it is intuitive that Lys-97_Y will contribute more to the free energy of complex formation than Lys-96_Y. Furthermore, in all three complexes, the side chain of Lys-97_Y is buried to a larger extent than Lys-96_Y, upon complex

TABLE 6 Surface area buried upon antibody-HEL complex formation of residues Lys-96_Y and Lys-97_Y

		Area buried upon complex formation			
Residue	Atom	HH8-HEL	HH10-HEL	HH10Fv-HEL	HH26-HEL
Lys-96_Y	N	–	–	–	–
	Cα	–	–	–	–
	C	0.33	0.59	0.06	0.34
	O	0.37	0.55	–	0.50
	Cβ	7.12	8.65	5.78	6.55
	Cγ	–	–	–	–
	Cδ	9.46	12.16	9.16	10.51
	Cε	0.10	–	–	0.47
	Nζ	38.87	37.23	37.98	29.24
Total buried		56.27	59.19	52.99	47.61
Lys-97_Y	N	0.38	0.21	0.35	0.12
	Cα	5.44	3.66	4.68	4.39
	C	–	–	–	–
	O	2.11	3.56	2.95	2.34
	Cβ	5.91	0.77	7.36	4.41
	Cγ	17.12	1.13	10.45	13.15
	Cδ	10.05	21.21	12.22	9.49
	Cε	27.46	33.39	25.93	24.88
	Nζ	39.22	33.94	38.87	51.53
Total buried		107.70	97.86	102.81	110.32

Listing of the buried surface areas of the atoms of Lys-96_Y and Lys-97_Y epitope residues upon the complex formation in HH8-HEL, HH10-HEL, HH10Fv-HEL, and HH26-HEL.
Atoms and their positions are shown in standard codes.
Last row in each is the sum of buried areas of all the atoms in the residue.

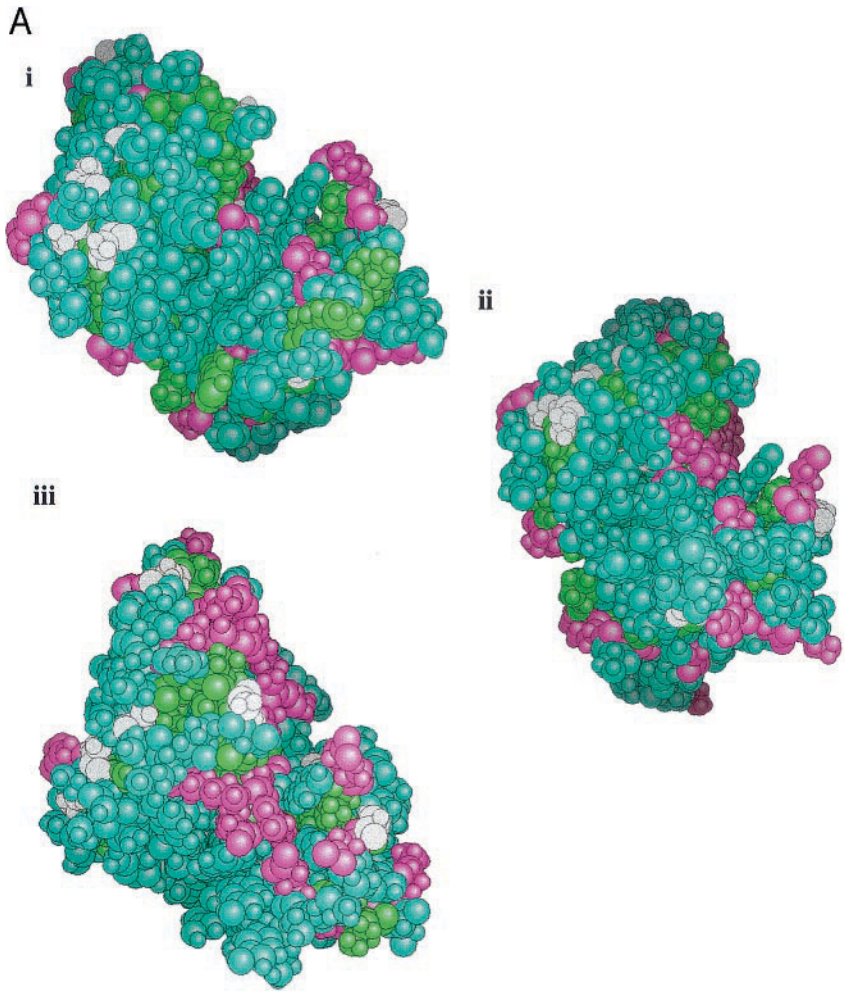

FIGURE 7 Electrostatic and hydrophobic properties of HH-HEL complexes. The binding sites of antibodies are shown. (*a*) The surface area types: *i*, HH8; *ii*, HH10; *iii*, HH26. Hydrophobic, polar, and charged residues are shown in green, cyan, and magenta, respectively. The figure has been generated using GRASP (Nicholls et al., 1991). (*b*) The components of residual potential of HH10-HEL. *i*, HEL interaction potential projected onto HH10; *ii*, HH10 desolvation potential. (*bi*) and (*bii*) are generated using GRASP (Nicholls et al., 1991), using the method by Tidor and coworkers (Chong et al., 1998; Lee and Tidor, 2001). For electrostatic complementarity, the two components of the residual potential should be equal and opposite (Chong et al., 1998; Lee and Tidor, 2001).

formation (Table 6). HH26-HEL complex buries the largest surface area of Lys-97_Y–Nζ atom among the three complexes (Table 6). The Nζ atoms of Lys-96_Y are buried to similar extents in the three complexes. The more a side chain is buried in the protein interior the higher desolvation penalty it pays (Novotny and Sharp, 1992; Bruccoleri et al., 1997). However, in the protein interior, due to the absence of solvent screening, the charged side chain will have very favorable electrostatic interactions if the protein environment permits. Strong salt bridges are usually buried in the protein interior (Kumar and Nussinov, 1999). This further suggests that the free energy of binding in the three complexes derives larger amounts from Lys-97_Y than from Lys-96_Y.

DISCUSSION

The significance of this work is that the observed variations in the electrostatic properties of the three antibodies correlate with their binding properties. The high number of short-range electrostatic interactions, very strong salt bridges and a very strong salt-bridge pentad at the binding site, and the largest electrostatic contributions toward binding in HH26-HEL, limit flexibility, rendering the binding site geometry very rigid. Consequently, the epitope mutations are not accommodated due to very limited conformational flexibility, or geometrical adaptability. In contrast, the small number of electrostatic interactions, marginal strengths of binding-site salt bridges, and small electrostatic contributions toward binding in HH8-HEL, allow conformational flexibility with less specific geometrical constrains at the binding site. Thus this antibody accommodates epitope mutations and is cross-reactive. HH10-HEL has intermediate electrostatic properties, both in terms of number of short-range electrostatic interactions and electrostatic contributions. Therefore, its binding properties relating to conformational flexibility and specificity also fall among the three antibodies.

The differential impacts of charge mutations on the association steps of the complexes suggest mechanisms of associations in the three HH-HEL complexes. Three important conclusions can be drawn from the observations. First, the variations in electrostatic versus hydrophobic interactions correlate with, and can account for, many of the

B

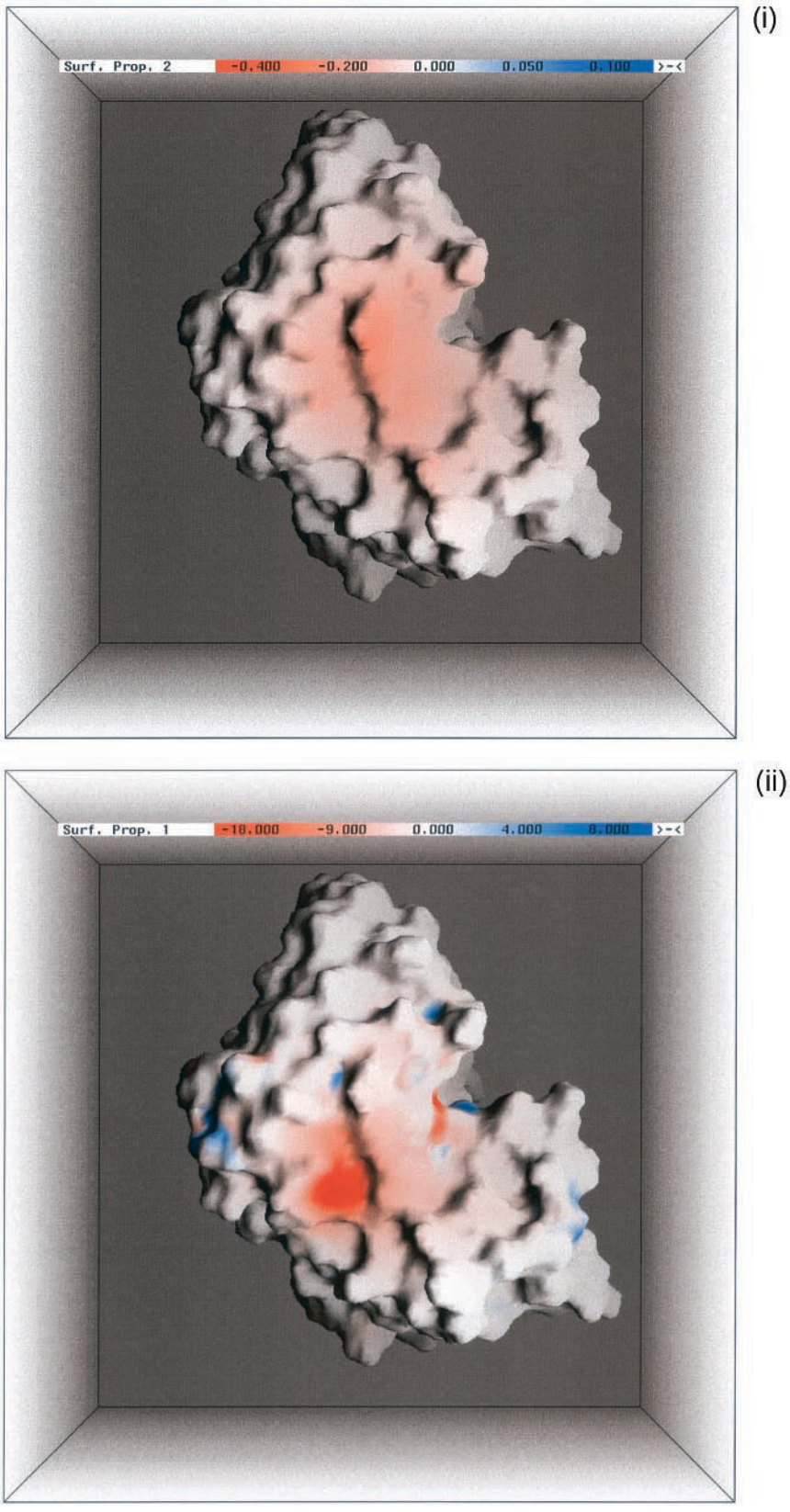
(i)
Surf. Prop. 2
-0.400
-0.200
0.000
0.050
0.100
(ii)
Surf. Prop. 1
-18.000
-9.000
0.000
4.000
8.000

specificity and affinity differences among the antibodies. Second, electrostatic interactions play duo roles, directly, by affecting specificity and affinity through complementary polar and charged based intermolecular contacts at the binding interface, and indirectly, on structural effects, through stabilizing the partners and their complexes, and modulating flexibility properties of the antibodies. Third, electrostatic effects that could be interpreted as diffusional electrostatic steering effects on the initial association process are actually interactions that are taking place after collision, which alter the stabilities of the encounter complexes and the transition-state energies of both encounter and docking steps.

The networked salt bridges, especially Glu-99_H–Lys-97_Y, Arg-97_H–Glu-99_H, and Arg-97_H–Asp-101_H in HH26-HEL, stand as very strong, even when compared with the strengths of very stabilizing salt bridges reported in literature (Lounnas and Wade, 1997; Kumar and Nussinov, 1999). This agrees with the observation that networked salt bridges, ion pairs, and hydrogen bonds are usually stabilizing (Kumar and Nussinov, 1999; Xiao and Honig, 1999; Sheinerman et al., 2000). In addition, the overall electrostatic contributions to the binding energy among the wild type and mutant complexes span a wide range. The range of the electrostatic term spans 20 kcal/mol, compared to the range of less than 4 kcal/mol for the hydrophobic term. The optimization of electrostatic interactions leads to specificity and tight binding (Sheinerman et al., 2000; Lee and Tidor, 2001). For such associations, the hydrophobicity may be optimized to begin with, whereas enhancement in electrostatic properties leads to a tight binding (Chong et al., 1999). Our results are consistent with these findings. The hydrophobic contributions are similar in all the complexes, with little variations. The high specificity of HH26 is acquired by the enhancement of its electrostatic properties during affinity maturation.

Our results are consistent with the conclusion that the net electrostatic component of the binding free energy is usually unfavorable (Table 5: sum of desolvation penalty and electrostatic interaction) because the unfavorable change in the electrostatics of solvation is not fully compensated by favorable electrostatics interactions of the bound complex (Novotny and Sharp, 1992; Bruccoleri et al., 1997). The compensation is greatest in HH26-HEL (30.5 kcal/mol), poorest in HH8-HEL (36.8 kcal/mol), and intermediate in HH10-HEL (34.8 kcal/mol). The optimized compensations between charge desolvation and favorable electrostatic interactions lead to specific binding, as shown from our analysis and from previous studies (Chong et al., 1999; Lee and Tidor, 2001). Here, it is important to emphasize the distinction between the overall electrostatic contributions and the local electrostatic contributions through the binding-site salt bridges. The overall electrostatic contributions mainly depend on proportion and distribution of charges and influences the strengths of local interactions. The favorable electrostatic term contributes the most in HH26-HEL, and least in HH8-HEL (Table 5), indicating further that HH26-HEL binding is electrostatically driven. Electrostatic interactions reflect primarily the enthalpic component of association, and our results agree with ITC studies, which show that, among the three complexes, HH26-HEL binding is the most enthalpically driven (S. Mohan, unpublished).

The three antibodies exhibit differential sensitivity to most mutations in the HEL epitope, with HH26 being the most sensitive and HH8 the least (Lavoie et al., 1999; Li et al., 2001). The differences in the number of charged residues versus hydrophobic residues in their respective binding site can explain many of these specificity differences (Fig. 7). Charged residues contribute to higher specificity globally through the electrostatic contribution to the free energy of binding, and locally by forming salt bridges, and their networks. It is expected that, for binding that is strongly electrostatic in nature, mutating the charged residues will leave rather severe effects on antibody–antigen associations, whereas mutating a hydrophobic residue would be less severe. However, because the HH26-HEL binding interface is expected to be rigid, where the binding site of HH26 is pre-organized with a specific geometry, any type of mutation will have a more severe affect on HH26-HEL binding than for HH8-HEL or HH10-HEL binding. This also agrees with the observation that the effects of mutations are modulated through the flexible regions of proteins (Sinha and Nussinov, 2001).

Particularly interesting is the presence of a strong intramolecular salt bridge, Asp-48_Y–Arg-61_Y, at the HH26-HEL binding site. This interaction is present in the uncomplexed HEL but is absent in HH8-HEL and HH10-HEL complexes. In HH8-HEL and HH10-HEL, the charged groups of the two residues, which form the salt bridge in HH26-HEL, are not oriented optimally to form a salt bridge, an indication of conformational adjustments upon lysozyme binding. Preservation of an intramolecular salt bridge of HEL upon HH26 association suggests a fine specificity of the HH26 binding site for its epitope, where binding-site geometry of HEL seems to be unaltered upon HH26 encounter and docking. This also suggests that HH26-HEL binding is more of a "lock and key" type, whereas, in HH8-HEL, the binding seems to be more like "induced fit" and HH10-HEL is intermediate. This salt bridge is also present in HH10Fv-HEL complex (Tables 2 and 3). However, the electrostatic strength of this salt bridge in HH10Fv-HEL is nearly neutral (Table 3).

The hydrophobic component of binding is more favorable in HH8-HEL than in HH10-HEL or HH26-HEL (Table 5). Hydrophobic and local folding effects account for most of the total entropy change of association (Spolar and Record, 1994). Isothermal titration calorimetry and SPR results show that HH8-HEL binding is entropically driven. The observed entropy would include hydrophobicity and local folding effects. The differences in binding properties of the three HH antibodies are mainly due to the differences in

their electrostatic components, consistent with an earlier report (Sharp, 1998).

Entropy–enthalpy compensation is fundamental to protein–protein associations, and is demonstrated experimentally (Bhat et al., 1994; Fields et al., 1996). Most protein–protein associations, including antibody–protein complexes, are enthalpically driven (Chong et al., 1999), and accompanied by a large unfavorable entropic change (Tamura and Privalov, 1997). Our data show large electrostatic and hydrophobic contributions to the antibody–HEL associations with larger differences among the complexes in electrostatic component. The number of electrostatic interactions, and their strengths, determining these features, in fact are the predispositions of protein environments, which stem from subtle evolutionary changes in protein sequence.

Electrostatic steering is likely a significant contributor to the stability of the encounter complex in all three antibodies, and, subsequently, to specific docking and determination of affinity. This is indicated by the slight slowing of the initial association rate constant k_{+1} in the complexes of all three antibodies with K97A. However, the magnitude of the change in k_{+1} was similar in all three antibodies. The mutation had a much greater impact on the transition state and stability of the encounter complexes and on docking, properties that would reflect post-collision events. Brownian dynamics simulations indicated that electrostatic steering interactions in HH10-HEL pair are weak and that the electrostatically favored orientation gives a mismatch of $\sim$180° rotation from the orientation in the crystal structure (Gabdoulline and Wade, 2001). This may explain why the mutation HEL(K96A) actually has favorable changes in some of the interaction steps. Our results with HEL(K97A) mutation are also consistent with this conclusion, and suggest that the effects of electrostatics on the apparent association rates, often interpreted as electrostatically enhanced diffusion, actually reflect later, specific interactions stabilizing the receptor and ligand complex, at least in these antibody–antigen complexes.

There seem to be two general mechanisms of electrostatic steering in protein–protein association. One, the common view, where the electrostatic steering brings the two proteins of the complex together (Schreiber and Fersht, 1996; Gabdoulline and Wade, 2001; Lee and Tidor, 2001). The electrostatic forces act here at pre-collision level, and enhance diffusional encounter (Gabdoulline and Wade, 2001). Such examples include barnase-barstar, acetylcholinesterase-fasculin-2, and cytochrome *c* peroxidase–cytochrome *c* complexes (Gabdoulline and Wade, 2001). The proteins in such complexes would show overall electrostatic complementarity at their binding sites, and additionally can have short-range intermolecular electrostatic interactions in docked complexes (Chong et al., 1998; Lee and Tidor, 2001). In the other type of apparent electrostatic steering, an alternative view, as in these three complexes, the electrostatic forces mainly act post-collision, and provide stability and specificity through the salt bridge and their networks. The proteins in such complexes may not show overall electrostatic complementarity at their binding sites (Fig. 7). This corresponds to the finding that electrostatically favorable orientations in HH5-HEL and HH10-HEL complexes are found to be significantly different from their actual bound complexes (Gabdoulline and Wade, 2001).

High-affinity antibodies have higher binding energies for their antigens (Patten et al., 1996; Wedemayer et al., 1997; Chong et al., 1999). Our data suggest that affinity maturation of HH8 and HH26 toward HEL may be via two independent mechanisms, where it is hydrophobically driven in one case and electrostatically in the other. It has been hypothesized that association rates are optimized early in affinity maturation (Foote and Milstein, 1994). Our results suggest that apparent increases in association rates may actually involve optimization of post-collision process, which also affect docking and complex stability. Thus, similar structural mechanisms may underly optimization of several steps of the binding process.

The continuum electrostatic model may not provide accurate quantitative values, because it does not take into account the local polarities in proteins resulting from permanent dipoles (Warshel et al., 1984). However, for qualitative comparisons, especially when experimental varifications are available, this widely used (Hendsch and Tidor, 1994; Xu et al., 1997a; Lounnas and Wade, 1997; Sinha et al., 2001a) and experimentally supported (Waldburger et al., 1995, 1996) method is of choice.

The calculations on theoretical models of HH8-HEL and HH26-HEL complexes might have affected the estimated values. However, it would not affect our conclusions for the following reasons: 1) Theoretical models were built from the template of more than 95% sequence identity; 2) The conclusions are consistent with the previously reported experimental findings; 3) The conclusions from our binding kinetics analysis and calculations correspond with each other; and 4) The conclusions are based on qualitative comparisons between the three complexes. The crystal structures of HH26-HEL and a chimera of Heavy-chain-8 and Light-chain-10 complexed with HEL will soon become available (Y. Li and R. Mariuzza, personal communication). These finding will be further verified.

CONCLUSIONS

The electrostatics contribute both globally and locally to protein–protein associations. Locally, electrostatic interactions, both structurally and thermodynamically, play major roles in determining specificity and affinity by limiting conformational flexibility, as in HH26. In contrast, lack of significant electrostatic interactions and their weak electrostatic contributions in HH8 render the binding site conformationally flexible, allowing higher cross-reactivity with mutant antigens. Intra- and intermolecular salt bridges and

their networks play major roles in defining specificity and affinity in HH26-HEL complex. Globally, the proportion and distributions of charged residues determine the overall electrostatic contributions toward binding and define the extent of electrostatic environment in protein. The higher number of binding-site-charged residues in HH26 results in higher overall electrostatic contributions toward binding.

Our results also indicate that apparent "electrostatic steering," measurable as an apparent enhancement of the initial association rate, may actually reflect two contrasting effects. The generally accepted phenomenon of electrostatic steering is enhancement of diffusional encounter through what is generally believed to be a long-range interaction. However, apparent enhancement of initial association rates may also reflect specific and local electrostatic interactions, which stabilize the initial encounter complex through binding-site ionic interactions and strong salt bridges. The apparent association rate is accelerated because there is minimal dissociation of the encounter complex. Our results with site-directed mutants of two charged epitope residues, Lys-96_Y and Lys-97_Y suggest that both residues equivalently affect long-range steering, but that only Lys-97_Y mediates post-collision stabilization through the formation of an intermolecular salt bridge and by participating in a salt-bridge network. In contrast, Lys-96_Y is not involved in any salt-bridge formation, and, in fact, faces away from the binding site. The measurable contributions of post-collision interactions to the total binding energy are much higher than long-range steering effects in both HH26-HEL and HH10-HEL complexes. Thus, mutational evidence of apparent electrostatic steering must be interpreted in light of both the binding kinetics and an analysis of the underlying electrostatic interactions to determine the actual mechanism of action.

APPENDIX

Listing of hydrogen bonds present in CDRs and epitopes of HH8-HEL, HH10-HEL, and HH26-HEL complexes. Hydrogen bond-forming residues are shown. The residue name is followed by its position, which is followed by chain identification in subscripts. Intra- and intermolecular hydrogen bonds are marked.

Complex	H-bond type*	H-bond	Corresponding Regions	Intra-molecular	Inter-molecular
HyHEL8	MC-MC	Ser-35_H–Ala-96_H	CDR1-Frame	✓	
		Phe-53_H–Gly-55_H	CDR2-CDR2	✓	
		Phe-53_H–Asn-56_H	CDR2-CDR2	✓	
		Asn-60_H–Leu-63_H	CDR2-CDR2	✓	
		Pro-61_H–Lys-64_H	CDR2-CDR2	✓	
		Leu-63_H–Arg-66_H	CDR2-Frame	✓	
		Asn-97_H–Gly-100_H	Frame-CDR3	✓	
		Thr-5_L–Arg-24_L	Frame-CDR1	✓	
		Thr-5_L–Arg-24_L	Frame-CDR1	✓	
		Ile-29_L–Asn-31_L	Frame-CDR1	✓	
		Ile-29_L–Gly-68_L	CDR1-Frame	✓	
		Ile-55_L–Gly-57_L	CDR2-Frame	✓	
		Ala-9_Y–Lys-13_Y	Epitope	✓	
		Ala-10_Y–Lys-13_Y	Epitope	✓	
		Lys-13_Y–Gly-16_Y	Epitope	✓	
		Tyr-20_Y–Tyr-2_Y	Epitope	✓	
		Trp-62_Y–Leu-75_Y	Epitope	✓	
		Trp-63_Y–Cys-76_Y	Epitope	✓	
		Thr-89_Y–Val-92_Y	Epitope	✓	
		Ala-90_Y–Asn-93_Y	Epitope	✓	
		Asn-93_Y–Lys-96_Y	Epitope	✓	
		Cys-94_Y–Lys-97_Y	Epitope	✓	
		Lys-97_Y–Ser-100_Y	Epitope	✓	
		Ile-98_Y–Asp-101_Y	Epitope	✓	
	MC-SC	Ile-29_H–Trp-34_H	Frame-CDR1	✓	
		Asp-32_H–Tyr-33_H	CDR1-CDR1	✓	
		Tyr-47_H–Asn-60_H	Frame-CDR2	✓	
		Glu-49_H–Tyr-50_H	Frame-CDR2	✓	
		Glu-49_H–Ile-51_H	Frame-CDR2	✓	
		Ser-52_H–Arg-71_H	CDR2-Frame	✓	
		Ser-52_H–Phe-53_H	CDR2-CDR2	✓	
		Ser-52_H–Asn-56_H	CDR2-CDR2	✓	
		Asn-56_H–Thr-57_H	CDR2-CDR2	✓	
		Phe-58_H–Trp-94_L	CDR2-Frame	✓	
		Tyr-59_H–Trp-94_L	CDR2-Frame	✓	
		Asn-60_H–Pro-61_H	CDR2-CDR2	✓	
		Asn-60_H–Ser-62_H	CDR2-CDR2	✓	
		Ser-62_H–Lys-64_H	CDR2-CDR2	✓	
		Leu-63_H–Arg-66_H	CDR2-Frame	✓	
		Asp-99_H–Gly-100_H	CDR3-CDR3	✓	
		Gly-100_H–Trp-103_H	CDR3-Frame	✓	
		Val-3_L–Ser-26_L	Frame-CDR1	✓	
		Gln-27_L–Ser-28_L	CDR1-CDR1	✓	
		Gly-30_L–Asn-92_L	CDR1-CDR3	✓	
		Gly-30_L–Asn-32_L	CDR1-CDR1	✓	
		Asn-31_L–Gly-16_Y	CDR1-Epitope		✓
		Asn-31_L–Arg-14_Y	CDR1-Epitope		✓
		Thr-49_L–Tyr-50_L	Frame-CDR2	✓	
		Gln-90_L–Asn-92_L	CDR3-CDR3	✓	
		Gln-90_L–Asn-93_L	CDR3-CDR3	✓	
		Gln-90_L–Asn-93_L	CDR3-CDR3	✓	
		Gln-90_L–Pro-95_L	CDR3-CDR3	✓	
		Gln-16_Y–Lys-96_Y	Epitope	✓	
		Asp-18_Y–Asn-19_Y	Epitope	✓	
		Asp-18_Y–Leu-25_Y	Epitope	✓	
		Asp-48_Y–Gly-49_Y	Epitope	✓	
		Asp-48_Y–Ser-50_Y	Epitope	✓	
		Trp-63_Y–Asn-74_Y	Epitope	✓	
		Asp-87_Y–Thr-89_Y	Epitope	✓	
		Asp-101_Y–Asn-103_Y	Epitope	✓	
		Asp-101_Y–Gly-104_Y	Epitope	✓	
	SC-SC	Tyr-50_H–Arg-21_Y	CDR2-Epitope		✓
		Asn-32_L–Asn-92_L	CDR1-CDR3	✓	
		Asn-92_L–Asn-93_L	CDR3-CDR3	✓	
HyHEL10	MC-MC	Tyr-33_H–Trp-98_H	CDR1-Frame	✓	
		Trp-34_H–Val-51_H	CDR1-CDR2	✓	
		Ser-35_H–Ala-96_H	CDR1-Frame	✓	
		Met-48_H–Asn-60_H	Frame-CDR2	✓	
		Tyr-50_H–Tyr-58_H	CDR2-CDR2	✓	
		Ser-52_H–Ser-56_H	CDR2-CDR2	✓	
		Ser-52_H–Gly-55_H	CDR2-CDR2	✓	
		Ser-52_H–Ser-56_H	CDR2-CDR2	✓	
		Tyr-53_H–Ser-56_H	CDR2-CDR2	✓	
		Asn-60_H–Leu-63_H	CDR2-CDR2	✓	
		Pro-61_H–Lys-64_H	CDR2-CDR2	✓	
		Thr-5_L–Arg-24_L	Frame-CDR1	✓	
		Thr-5_L–Arg-24_L	Frame-CDR1	✓	
		Ile-29_L–Gly-68_L	CDR1-Frame	✓	
		Gly-30_L–Gly-68_L	CDR1-Frame	✓	
		Leu-33_L–Tyr-50_L	CDR1-CDR2	✓	
		Leu-33_L–Tyr-50_L	CDR1-CDR2	✓	
		His-34_L–Gly-89_L	CDR1-CDR3	✓	
		His-34_L–Gln-89_L	CDR1-CDR3	✓	
		Lys-49_L–Gln-53_L	Frame-CDR2	✓	
		Lys-49_L–Ser-52_L	Frame-CDR2	✓	
		Lys-49_L–Gln-53_L	Frame-CDR2	✓	
		Pro-95_L–Thr-97_L	CDR3-Frame	✓	
		Ala-10_Y–Lys-13_Y	Epitope	✓	

Complex	H-bond type*	H-bond	Corresponding Regions	Intra-molecular	Inter-molecular
		$Lys\text{-}13_Y$–$Gly\text{-}16_Y$	Epitope	✓	
		$Leu\text{-}17_Y$–$Tyr\text{-}20_Y$	Epitope	✓	
		$Tyr\text{-}20_Y$–$Tyr\text{-}23_Y$	Epitope	✓	
		$Tyr\text{-}20_Y$–$Tyr\text{-}23_Y$	Epitope	✓	
		$Trp\text{-}63_Y$–$Leu\text{-}75_Y$	Epitope	✓	
		$Trp\text{-}63_Y$–$Cys\text{-}76_Y$	Epitope	✓	
		$Thr\text{-}89_Y$–$Val\text{-}92_Y$	Epitope	✓	
		$Asn\text{-}93_Y$–$Lys\text{-}96_Y$	Epitope	✓	
		$Cys\text{-}94_Y$–$Lys\text{-}97_Y$	Epitope	✓	
		$Lys\text{-}97_Y$–$Ser\text{-}100_Y$	Epitope	✓	
		$Ile\text{-}98_Y$–$Asp\text{-}101_Y$	Epitope	✓	
	MC-SC	$Ile\text{-}29_H$–$Trp\text{-}34_H$	Frame-CDR1	✓	
		$Thr\text{-}30_H$–$Ser\text{-}31_H$	Frame-CDR1	✓	
		$Asp\text{-}32_H$–$Trp\text{-}34_H$	CDR1-CDR1	✓	
		$Asp\text{-}32_H$–$Tyr\text{-}33_H$	CDR1-CDR1	✓	
		$Tyr\text{-}47_H$–$Asn\text{-}60_H$	Frame-CDR2	✓	
		$Tyr\text{-}59_H$–$Trp\text{-}94_L$	CDR2-CDR3	✓	
		$Tyr\text{-}59_H$–$Ile\text{-}69_H$	CDR2-Frame	✓	
		$Asn\text{-}60_H$–$Pro\text{-}61_H$	CDR2-CDR2	✓	
		$Asn\text{-}60_H$–$Ser\text{-}62_H$	CDR2-CDR2	✓	
		$Asn\text{-}97_H$–$Tyr\text{-}102_H$	Frame-CDR3	✓	
		$Gly\text{-}100_H$–$Trp\text{-}103_H$	CDR3-Frame	✓	
		$Val\text{-}3_L$–$Ser\text{-}26_L$	Frame-CDR1	✓	
		$Ser\text{-}26_L$–$Gln\text{-}27_L$	CDR1-CDR1	✓	
		$Gly\text{-}30_L$–$Asn\text{-}32_L$	CDR1-CDR1	✓	
		$Gly\text{-}30_L$–$Asn\text{-}31_L$	CDR1-CDR1	✓	
		$Asn\text{-}31_L$–$Asn\text{-}32_L$	CDR1-CDR1	✓	
		$Asn\text{-}31_L$–$Gly\text{-}16_Y$	CDR1-Epitope		✓
		$Asn\text{-}32_L$–$Gly\text{-}16_Y$	CDR1-Epitope		✓
		$Gln\text{-}89_L$–$Gln\text{-}90_L$	CDR3-CDR3	✓	
		$Gln\text{-}90_L$–$Ser\text{-}93_L$	CDR3-CDR3	✓	
		$Gln\text{-}90_L$–$Pro\text{-}95_L$	CDR3-CDR3	✓	
		$Asn\text{-}92_L$–$Asn\text{-}19_Y$	CDR3-Epitope		✓
		$His\text{-}15_Y$–$Lys\text{-}96_Y$	Epitope	✓	
		$Asp\text{-}18_Y$–$Asn\text{-}19_Y$	Epitope	✓	
		$Asp\text{-}18_Y$–$Asn\text{-}19_Y$	Epitope	✓	
		$Asp\text{-}48_Y$–$Gly\text{-}49_Y$	Epitope	✓	
		$Asp\text{-}48_Y$–$Ser\text{-}50_Y$	Epitope	✓	
		$Trp\text{-}63_Y$–$Asn\text{-}74_Y$	Epitope	✓	
		$Asp\text{-}87_Y$–$Thr\text{-}89_Y$	Epitope	✓	
		$Asp\text{-}101_Y$–$Gly\text{-}102_Y$	Epitope	✓	
		$Asp\text{-}101_Y$–$Asn\text{-}103_Y$	Epitope	✓	
	SC-SC	$Tyr\text{-}50_H$–$Arg\text{-}21_Y$	CDR2-Epitope		✓
		$Tyr\text{-}50_H$–$Arg\text{-}21_Y$	CDR2-Epitope		✓
		$Asp\text{-}99_H$–$His\text{-}34_L$	CDR2-Frame	✓	
		$Asn\text{-}32_L$–$Asn\text{-}92_L$	CDR1-CDR3	✓	
		$Gln\text{-}53_L$–$Asn\text{-}93_Y$	CDR2-Epitope	✓	
HyHEL26	MC-MC	$Trp\text{-}34_H$–$Ile\text{-}51_H$	CDR1-CDR2	✓	
		$Trp\text{-}34_H$–$Ile\text{-}51_H$	CDR1-CDR2	✓	
		$Ser\text{-}35_H$–$Ala\text{-}96_H$	CDR1-Frame	✓	
		$Met\text{-}48_H$–$Asn\text{-}60_H$	Frame-CDR2	✓	
		$Ser\text{-}52_H$–$Ser\text{-}56_H$	CDR2-CDR2	✓	
		$Ser\text{-}52_H$–$Gly\text{-}55_H$	CDR2-CDR2	✓	
		$Ser\text{-}52_H$–$Ser\text{-}56_H$	CDR2-CDR2	✓	
		$Asn\text{-}60_H$–$Leu\text{-}63_H$	CDR2-CDR2	✓	
		$Pro\text{-}61_H$–$Lys\text{-}64_H$	CDR2-CDR2	✓	
		$Leu\text{-}63_H$–$Arg\text{-}66_H$	CDR2-Frame	✓	
		$Arg\text{-}97_H$–$Met\text{-}100_H$	Frame-CDR3	✓	
		$Thr\text{-}5_L$–$Arg\text{-}24_L$	Frame-CDR1	✓	
		$Ile\text{-}29_L$–$Gly\text{-}68_L$	CDR1-Frame	✓	
		$Ile\text{-}29_L$–$Gly\text{-}68_L$	CDR1-Frame	✓	
		$Asn\text{-}32_L$–$Ser\text{-}91_L$	CDR1-CDR3	✓	
		$Leu\text{-}33_L$–$Tyr\text{-}50_L$	CDR1-CDR2	✓	
		$Leu\text{-}33_L$–$Tyr\text{-}50_L$	CDR1-CDR2	✓	
		$Leu\text{-}47_L$–$Ile\text{-}55_L$	Frame-CDR2	✓	
		$Lys\text{-}49_L$–$Ala\text{-}51_L$	Frame-CDR2	✓	
		$Lys\text{-}49_L$–$Gln\text{-}53_L$	Frame-CDR2	✓	
		$Asn\text{-}92_L$–$Arg\text{-}21_Y$	CDR3-Epitope		✓
		$Ala\text{-}10_Y$–$Lys\text{-}13_Y$	Epitope	✓	
		$Lys\text{-}13_Y$–$Gly\text{-}16_Y$	Epitope	✓	
		$Leu\text{-}17_Y$–$Tyr\text{-}20_Y$	Epitope	✓	
		$Tyr\text{-}20_Y$–$Tyr\text{-}23_Y$	Epitope	✓	
		$Tyr\text{-}20_Y$–$Tyr\text{-}23_Y$	Epitope	✓	
		$Trp\text{-}62_Y$–$Leu\text{-}75_Y$	Epitope	✓	
		$Trp\text{-}63_Y$–$Leu\text{-}75_Y$	Epitope	✓	
		$Thr\text{-}89_Y$–$Val\text{-}92_Y$	Epitope	✓	
		$Ala\text{-}90_Y$–$Asn\text{-}93_Y$	Epitope	✓	
		$Asn\text{-}93_Y$–$Lys\text{-}96_Y$	Epitope	✓	
		$Asn\text{-}93_Y$–$Lys\text{-}97_Y$	Epitope	✓	
		$Cys\text{-}94_Y$–$Lys\text{-}97_Y$	Epitope	✓	
		$Lys\text{-}97_Y$–$Ser\text{-}100_Y$	Epitope	✓	
		$Ile\text{-}98_Y$–$Asp\text{-}101_Y$	Epitope	✓	
	MC-SC	$Val\text{-}2_H$–$Tyr\text{-}102_H$	Frame-CDR3	✓	
		$Ile\text{-}29_H$–$Trp\text{-}34_H$	Frame-CDR1	✓	
		$Asp\text{-}32_H$–$Trp\text{-}34_H$	CDR1-CDR1	✓	
		$Asp\text{-}32_H$–$Arg\text{-}71_H$	CDR1-Frame	✓	
		$Ile\text{-}51_H$–$Arg\text{-}71_H$	CDR2-Frame	✓	
		$Tyr\text{-}59_H$–$Trp\text{-}94_L$	CDR2-CDR3	✓	
		$Tyr\text{-}59_H$–$Ile\text{-}69_H$	CDR2-Frame	✓	
		$Asn\text{-}60_H$–$Pro\text{-}61_H$	CDR2-CDR2	✓	
		$Asn\text{-}60_H$–$Ser\text{-}62_H$	CDR2-CDR2	✓	
		$Met\text{-}100_H$–$Trp\text{-}103_H$	CDR3-Frame	✓	
		$Asp\text{-}101_H$–$Tyr\text{-}102_H$	CDR3-Frame	✓	
		$Gln\text{-}27_L$–$Ser\text{-}28_L$	CDR1-CDR1	✓	
		$Ser\text{-}30_L$–$Asn\text{-}32_L$	CDR1-CDR1	✓	
		$Ser\text{-}30_L$–$Asn\text{-}31_L$	CDR1-CDR1	✓	
		$Asn\text{-}31_L$–$Arg\text{-}14_Y$	CDR1-Epitope		✓
		$Asn\text{-}32_L$–$Gly\text{-}16_Y$	CDR1-Epitope		✓
		$Ala\text{-}51_L$–$Gln\text{-}53_L$	CDR2-CDR2	✓	
		$Ser\text{-}52_L$–$Gln\text{-}53_L$	CDR2-CDR2	✓	
		$Ser\text{-}52_L$–$Gln\text{-}53_L$	CDR2-CDR2	✓	
		$Ser\text{-}54_L$–$Ile\text{-}55_L$	CDR2-CDR2	✓	
		$Ser\text{-}56_L$–$Gly\text{-}57_L$	CDR2-Frame	✓	
		$Gln\text{-}89_L$–$Tyr\text{-}96_L$	CDR3-CDR3	✓	
		$Gln\text{-}90_L$–$Asn\text{-}92_L$	CDR3-CDR3	✓	
		$Gln\text{-}90_L$–$Ser\text{-}93_L$	CDR3-CDR3	✓	
		$Gln\text{-}90_L$–$Ser\text{-}93_L$	CDR3-CDR3	✓	
		$Gln\text{-}90_L$–$Pro\text{-}95_L$	CDR3-CDR3	✓	
		$Asn\text{-}92_L$–$Arg\text{-}21_Y$	CDR3-Epitope		✓
		$Asn\text{-}92_L$–$Asn\text{-}19_Y$	CDR3-Epitope		✓
		$Ser\text{-}93_L$–$Trp\text{-}94_L$	CDR3-CDR3	✓	
		$Asn\text{-}18_Y$–$Asn\text{-}19_Y$	Epitope	✓	
		$Asp\text{-}48_Y$–$Arg\text{-}61_Y$	Epitope	✓	
		$Asp\text{-}48_Y$–$Gly\text{-}49_Y$	Epitope	✓	
		$Trp\text{-}63_Y$–$Asn\text{-}74_Y$	Epitope	✓	
		$Asp\text{-}87_Y$–$Thr\text{-}89_Y$	Epitope	✓	
		$Thr\text{-}89_Y$–$Asn\text{-}93_Y$	Epitope	✓	
		$Asp\text{-}101_Y$–$Gly\text{-}102_Y$	Epitope	✓	
		$Asp\text{-}101_Y$–$Asn\text{-}103_Y$	Epitope	✓	
	SC-SC	$Tyr\text{-}50_H$–$Arg\text{-}21_Y$	CDR2-Epitope		✓
		$Tyr\text{-}50_H$–$Arg\text{-}21_Y$	CDR2-Epitope		✓
		$Arg\text{-}97_H$–$Glu\text{-}99_H$	Frame-CDR3	✓	
		$His\text{-}15_Y$–$Thr\text{-}89_Y$	Epitope	✓	
		$Asp\text{-}18_Y$–$Asn\text{-}19_Y$	Epitope	✓	
		$Arg\text{-}21_Y$–$Ser\text{-}100_Y$	Epitope	✓	

*H-bond, hydrogen-bond; MC–MC, main chain–main chain; MC–SC, main chain–side chain; SC–SC, side chain–side chain; CDR, complementarity determining region.

We thank Prof. Ruth Nussinov for many helpful suggestions while preparing the manuscript. N.S. would also like to thank Dr. Sandeep Kumar for helpful discussions. Advanced Biomedical Computing Center personnel are thanked for computational resources, and related assistance. The personnel at National Cancer Institute–Frederick, MD are thanked for their assistance.

REFERENCES

Antosiewicz, J., and J. A. McCammon. 1995. Electrostatic and hydrodynamic orientational steering effects in enzyme–substrate association. *Biophys. J.* 69:57–65.

Barlow, D. J., and J. M. Thornton. 1983. Ion-pairs in proteins. *J. Mol. Biol.* 168:867–885.

Barre, S., A. S. Greenberg, M. F. Flajnik, and C. Chothia. 1994. Structural conservation of hypervariable regions in immunoglobulins evolution. *Nat. Struct. Biol.* 1:915–920.

Bernstein, F. C., T. F. Koetzle, G. H. Williams, E. E., Meyer, Jr., M. D. Brice, J. R. Rodgers, O. Kennard, T. Shimanouchi, and M. Tasumi. 1977. The Protein Data Bank: a computer-based archival file for macromolecular structures. *J. Mol. Biol.* 112:535–542.

Bhat, T. N., G. A. Bentley, G. Boulot, M. I. Greene, D. Tello, W. Dall'Acqua, H. Souchon, F. P. Schwarz, R. A. Mariuzza, and R. J. Poljak. 1994. Bound water molecules and conformational stabilization help mediate an antigen–antibody association. *Proc. Natl. Acad. Sci. U.S.A.* 91:1089–1093.

Braden, B. C., and R. J. Poljak. 1995. Structural features of the reactions between antibodies and protein antigens. *FASEB J.* 9:9–16.

Bruccoleri, R. E., J. Novotny, and M. E. Davis. 1997. Finite difference Poisson–Boltzman electrostatic calculations: increased accuracy achieved by harmonic dielectric smoothing and charge antialiasing. *J. Comput. Chem.* 18:268–276.

Chong, L. T., S. E. Dempster, Z. S. Hendsch, L. P. Lee, and B. Tidor. 1998. Computation of electrostatic complements to proteins: a case of charge stabilized binding. *Protein Sci.* 7:206–210.

Chong, L. T., Y. Duan, L. Wang, I. Massova, and P. A. Kollman. 1999. Molecular dynamics and free energy calculations applied to affinity maturation in antibody 48G7. *Proc. Natl. Acad. Sci. U.S.A.* 96: 14330–14335.

Chothia, C. 1974. Hydrophobic bonding and accessible surface area in proteins. *Nature.* 248:338–339.

Dall'Acqua, W., E. R. Goldman, W. Lin, C. Teng, D. Tsuchiya, H. Li, X. Ysern, B. C. Braden, Y. Li, S. J. Smith-Gill, and R. A. Mariuzza. 1998. A mutational analysis of binding interactions in an antigen–antibody protein–protein complex. *Biochemistry.* 37:7981–7991.

Diaw, L., C. Magnac, O. Pritsch, M. Buckle, P. M. Alzari, and G. Dighiero. 1997. Structural and affinity studies of IgM polyreactive natural autoantibodies. *J. Immunol.* 158:968–976.

Ditzel, H. J., K. Itoh, and D. R. Burton. 1996. Determinants of polyreactivity in a large panel of recombinant human antibodies from HIV-1 infection. *J. Immunol.* 157:739–749.

Eaton, B. E., L. Gold, and D. A. Zichi. 1995. Let's get specific: the relationship between specificity and affinity. *Chemistry and Biology.* 2:633–638.

Fields, B. A., F. A. Goldbaum, W. Dall'Acqua, E. L. Malchiodi, A. Cauerhff, F. P. Schwarz, X. Ysern, R. J. Poljak, and R. A. Mariuzza. 1996. Hydrogen-bonding and solvent structure in an antigen–antibody interface. Crystal structures and thermodynamic characterization of three Fv mutants complexed with lysozyme. *Biochemistry.* 35:15494–15503.

Foote, J., and C. Milstein. 1994. Conformational isomerism and the diversity of antibodies. *Proc. Natl. Acad. Sci. U.S.A.* 91:10370–10374.

Freire, E. 1999. The propagation of binding interactions to remote sites in proteins: analysis of the binding of the monoclonal antibody D1.3 to lysozyme. *Proc. Natl. Acad. Sci. U.S.A.* 96:10118–10122.

Gabdoulline, R. R., and R. C. Wade. 2001. Protein–protein association: investigation of factors influencing association rates by Brownian dynamics simulations. *J. Mol. Biol.* 306:1139–1155.

Gilson, M. K., and B. H. Honig. 1987. Calculation of electrostatic potential in an enzyme active site. *Nature.* 330:84–86.

Gilson, M. K., A. Rashin, R. Fine, and B. Honig. 1985. On the calculation of electrostatic interactions in proteins. *J. Mol. Biol.* 183:503–516.

Haselkorn, D., S. Friedman, D. Givol, and I. Pecht. 1974. Kinetic mapping of the antibody combining site by chemical relaxation spectrometry. *Biochemistry.* 13:2210–2222.

Hendsch, Z. S., and B. Tidor. 1994. Do salt-bridges stabilize proteins? A continuum electrostatic analysis. *Protein Sci.* 3:211–226.

Honig, B., and A. Nicholls. 1995. Classical electrostatics in biology and chemistry. *Science.* 268:1144–1149.

Jackson, R. M. 1999. Comparison of protein–protein interactions in serine protease-inhibitor and antibody–antigen complexes: Implications for the protein docking problem. *Protein Sci.* 8:603–613.

Janin, J. 1997. The kinetics of protein–protein recognition. *Proteins Struc. Func. Genet.* 28:153–161.

Kabat, E. A., T. T. Wu, and H. Bilofsky. 1977. Unusual distributions of amino acids in complementarity-determining (hyper-variable) segments of heavy and light chains of immunoglobulins and their possible roles in specificity of antibody-combining sites. *J. Biol. Chem.* 252:6609–6616.

Kangas, E., and B. Tidor. 2001. Electrostatic complementarity at ligand binding sites: application to chorismate mutase. *J. Phys. Chem. B.* 105: 880–888.

Kawaguchi, S., Y. Nobe, J. Yasuoka, T. Wakamiya, S. Kusumoto, and S. Kuramitsu. 1997. Enzyme flexibility: a new concept in recognition of hydrophobic substrates. *J. Biochem. (Tokyo).* 122:55–63.

Klapper, I., R. Hagstrom, R. Fine, K. Sharp, and B. Honig. 1986. Focusing of electric fields in the active site of Cu-Zn superoxide dismutase: effects ionic strength and amino acid modification. *Proteins Struc. Funct. Genet.* 1:47–59.

Krauss, G., D. Riesner, and G. Maass. 1976. Mechanism of discrimination between cognate and non-cognate tRNAs by phenylalanyl-tRNA synthetase from yeast. *Eur. J. Biochem.* 68:81–93.

Kumar, S., B. Ma, C. J. Tsai, and R. Nussinov. 2000. Electrostatic strengths of salt-bridges in thermophilic and mesophilic glutamate dehydrogenase monomers. *Proteins Struc. Fuct. Genet.* 38:368–383.

Kumar, S., and R. Nussinov. 1999. Salt-bridge stability in monomeric proteins. *J. Mol. Biol.* 293:1241–1255.

Kondoi, H., M. Shiroishi, M. Matsushima, K. Tsumoto, and I. Kumagai. 1999. Crystal structure of anti-hen egg white lysozyme antibody (HyHEL-10) Fv-antigen complex. Local structural changes in the protein antigen and water-mediated interactions of Fv–antigen and light chain–heavy chain interfaces. *J. Biol. Chem.* 274:27623–27631.

Kozack, R. E., M. J. d'Mello, and S. Subramaniam. 1995. Computer modeling of electrostatic steering and orientational effects in antibody-antigen association. *Biophys. J.* 68:807–814.

Lavoie, T. B., W. N. Drohan, and S. J. Smith-Gill. 1992. Experimental analysis by site-directed mutagenesis of somatic mutation effects on affinity and fine specificity in antibodies specific for lysozyme. *J. Immunol.* 148:503–513.

Lavoie, T. B., S. Mohan, C. A. Lipschultz, J.-C. Grivel, Y. Li, C. R. Mainhart, L. N. W. Kam-Morgan, W. N. Drohan, S. J. Smith-Gill. 1999. Structural differences among monoclonal antibodies with distinct fine specificities and kinetic properties. *Mol. Immonol.* 36:1189–1205.

Lee, B., and F. M. Richards. 1971. The interpretation of protein structures: estimation of static accessibility. *J. Mol. Biol.* 55:379–400.

Lee, C., and S. Subbiah. 1991. Prediction of protein side-chain conformation by packing optimization. *J. Mol. Biol.* 217:373–388.

Lee, L. P., and B. Tidor. 2001. Optimization of binding electrostatics: charge complementarity in the barnase-barstar protein complex. *Protein Sci.* 10:362–377.

Levitt, M. 1992. Accurate modeling of protein conformation by automatic segment matching. *J. Mol. Biol.* 226:507–533.

Li, Y., H. Li, S. J. Smith-Gill, and R. A. Mariuzza. 2000. Three-dimensional structures of the free and antigen-bound Fab from monoclonal antilysozyme antibody HyHEL-63. *Biochemistry.* 39:6296–6309.

Li, Y., C. A. Lipschultz, S. Mohan, and S. J. Smith-Gill. 2001. Mutations of an epitope hot-spot residue alter rate limiting steps of antigen–antibody protein–protein associations. *Biochemistry.* 40: 2011–2022.

Lindner, A. B., Z. Eshhar, and D. S. Tawfik. 1999. Conformational changes affect binding and catalysis by ester-hydrolysing antibodies. *J. Mol. Biol.* 285:421–430.

Lipschultz, C. A., Y. Li, and S. Smith-Gill. 2000. Experimental design for analysis of complex kinetics using surface plasmon resonance. *Methods.* 20:310–318.

Lounnas, V., and R. C. Wade. 1997. Exceptionally stable salt-bridges in cytochrome P450cam have functional roles. *Biochemistry.* 36: 5402–5417.

Marqusee, S., and R. T. Sauer. 1994. Contribution of a hydrogen-bond/salt-bridge network to the stability of secondary and tertiary structures in lambda repressor. *Protein Sci.* 3:2217–2225.

Mian, I. S., A. R. Bradwell, and A. J. Olson. 1991. Structure, function and properties of antibody binding sites. *J. Mol. Biol.* 217:133–151. Review.

Musafia, B., V. Buchner, and D. Arad. 1995. Complex salt-bridges in proteins: statistical analysis of structure and function. *J. Mol. Biol.* 254:761–770.

Musci, G., L. J. Berliner, and C. T. Esmon. 1988. Evidence for multiple conformational changes in the active center of thrombin induced by complex formation with thrombomodulin: an analysis employing nitroxide spin-labels. *Biochemistry.* 27:769–773.

Newman, M. A., C. R. Mainhart, C. P. Mallett, T. B. Lavoie, and S. J. Smith-Gill. 1992. Patterns of antibody specificity during the BALB/c immune response to hen eggwhite lysozyme. *J. Immunol.* 149: 3260–3272.

Nicholls, A., K. A. Sharp, and B. Honig. 1991. Protein folding and association: insights from the interfacial and thermodynamic properties of hydrocarbons. *Proteins Struc. Funct. Genet.* 11:281–296.

Nicholson, L. K., T. Yamazaki, D. A. Torchia, S. Grzesiek, A. Bax, S. J. Stahl, J. D. Kaufman, P. T. Wingfield, P. Y. Lam, P. K. Jadhav et al. 1995. Flexibility and function in HIV-1 protease. *Nat. Struct. Biol.* 2:274–280.

Novotny, J., R. E. Bruccoleri, and F. A. Saul. 1989. On the attribution of binding energy in antigen–antibody complexes McPC 603, D1.3, and HyHEL5. *Biochemistry.* 28:4735–4749.

Novotny, J., and K. Sharp. 1992. Electrostatic fields in antibodies and antibody/antigen complexes. *Prog. Biophys. Mol. Biol.* 58:203–224.

Padlan, E. A., E. W. Silverton, S. Sheriff, G. H. Cohen, S. J. Smith-Gill, and D. R. Davies. 1989. Structure of an antibody–antigen complex: crystal structure of the HyHEL-10 Fab-lysozyme complex. *Proc. Natl. Acad. Sci. U.S.A.* 86:5938–5942.

Patten, P. A., N. S. Gray, P. L. Yang, C. B. Marks, G. J. Wedemayer, J. J. Boniface, R. C. Stevens, and P. G. Schultz. 1996. The immunological evolution of catalysis. *Science.* 271:1086–1091.

Perutz, M. F. 1970. Stereochemistry of cooperative effects in haemoglobin. *Nature.* 228:726–739.

Pons, J., A. Rajpal, and J. F. Kirsch. 1999. Energetic analysis of an antigen/antibody interface: alanine scanning mutagenesis and double mutant cycles on the HyHEL-10/lysozyme interaction. *Protein Sci.* 8:958–968.

Rose, G. D., A. R. Geselowitz, G. J. Lesser, R. H. Lee, and M. H. Zehfus. 1985. Hydrophobicity of amino acid residues in globular proteins. *Science.* 229:834–838.

Ross, P. D., and S. Subramanian. 1981. Thermodynamics of protein association reactions: forces contributing to stability. *Biochemistry.* 20: 3096–3102.

Schreiber, G., and A. R. Fersht. 1996. Rapid, electrostatically assisted association of proteins. *Nat. Struct. Biol.* 3:427–431.

Selzer, T., and G. Schreiber. 2001. New insights into the mechanism of protein–protein association. *Proteins Struc. Funct. Genet.* 45:190–198.

Sharp, K. A. 1998. Calculation of HyHEL10-lysozyme binding free energy changes: effect of ten point mutations. *Proteins Struc. Func. Genet.* 33:39–48.

Sheinerman, F. B., R. Norel, and B. Honig. 2000. Electrostatic aspects of protein–protein interactions. *Curr. Opin. Struct. Biol.* 10:153–159. Review.

Sheriff, S., P. D. Jeffrey, and J. Bajorath. 1996. Comparison of CH1 domains in different classes of murine antibodies. *J. Mol. Biol.* 263: 385–389.

Sines, J. J., S. A. Allison, and J. A. McCammon. 1990. Point charge distributions and electrostatic steering in enzyme/substrate encounter: Brownian dynamics of modified copper/zinc superoxide dismutases. *Biochemistry.* 29:9403–9412.

Sinha, N., S. Kumar, and R. Nussinov. 2001a. Inter-domain interactions in hinge-bending transitions. *Struct. Fold. Design.*9:1165–1181.

Sinha, N., and R. Nussinov. 2001. Point mutations and sequence variability in proteins: redistributions of preexisting populations. *Proc. Natl. Acad. Sci. U.S.A.* 98:3139–3144.

Sinha, N., C. J. Tsai, and R. Nussinov. 2001b. A proposed structural model for amyloid fibril elongation: domain swapping forms an interdigitating-structure polymer. *Protein Eng.* 14:93–103.

Sitkoff, D., K. A. Sharp, and B. Honig. 1994. Accurate calculation of hydration free energies using macroscopic solvent models. *J. Phys. Chem.* 98:1978–1988.

Smith-Gill, S. J. 1991. Protein–protein interactions: structural motifs and molecular recognition. *Curr. Opin. Biotech.* 2:568–575.

Smith-Gill, S. J., C. Mainhart, T. B. Lavoie, R. J. Feldmann, W. Drohan, and B. R. Brooks. 1987. A three-dimensional model of an anti-lysozyme antibody. *J. Mol. Biol.* 194:713–724.

Spolar, R. S., and M. T. Record. 1994. Coupling of local folding to site-specific binding of proteins to DNA. *Science.* 263:777–784.

Sparrer, H., H. Lilie, and J. Buchner. 1996. Dynamics of the GroEL-protein complex: effects of nucleotides and folding mutants. *J. Mol. Biol.* 258: 74–87.

Sun, D. P., U. Sauer, H. Nicholson, and B. W. Matthews. 1991. Contributions of engineered surface salt-bridges to the stability of T4 lysozyme determined by directed mutagenesis. *Biochemistry.* 30:7142–7153.

Tamura, A., and P. L. Privalov. 1997. The entropy cost of protein association. *J. Mol. Biol.* 273:1048–1060.

Tsumoto, K., Y. Ueda, K. Maenaka, K. Watanabe, K. Ogasahara, K. Yutani, and I. Kumagai. 1994. Contribution to antibody–antigen interaction of structurally perturbed antigenic residues upon antibody binding. *J. Biol. Chem.* 269:28777–28782.

Wagner, G. 1995. The importance of being floppy. *Nat. Struct. Biol.* 2:255–257.

Waldburger, C. D., T. Jonsson, and R. T. Sauer. 1996. Barriers to protein folding: formation of buried polar interactions is a new slow step in acquisition of structure. *Biochemistry.* 93:2629–2634.

Waldburger, C. D., J. F. Schildback, and R. T. Sauer. 1995. Are buried salt-bridges important for protein stability and conformational specificity. *Nature Struc. Biol.* 2:122–128.

Walters, K. J., K. T. Dayie, R. J. Reece, M. Ptashne, and G. Wagner. 1997. Structure and mobility of the PUT3 dimer. *Nat. Struct. Biol.* 4:744–750.

Warshel, A., S. T. Russell, and A. K. Churg. 1984. Macroscopic models for studies of electrostatic interactions in proteins: limitations and applicability. *Proc. Natl. Acad. Sci. U.S.A.* 81:4785–4789.

Wedemayer, G. J., P. A. Patten, L. H. Wang, P. G. Schultz, and R. C. Stevens. 1997. Structural insights into the evolution of an antibody combining site. *Science.* 276:1665–1669.

Wilson, I. A., and R. L. Stanfield. 1993. Antibody–antigen interactions. *Curr. Opin. Struct. Biol.* 3:113–118.

Xiao, L., and B. Honig. 1999. Electrostatic contributions to the stability of hyper-thermophilic proteins. *J. Mol. Biol.* 289:1435–1444.

Xu, D., S. L. Lin, and R. Nussinov. 1997a. Protein binding versus protein folding: the role of hydrophilic bridges in protein associations. *J. Mol. Biol.* 265:68–84.

Xu, D., C. J. Tsai, and R. Nussinov. 1997b. Hydrogen bonds and salt bridges across protein–protein interfaces. *Protein Eng.* 10:999–1012.

Yip, K. S. P., K. L. Britton, T. J. Stillman, J. Lebbink, W. M. De Vos, F. T. Robb, C. Vetriani, D. Maeder, and D. W. Rice. 1998. Insights into the molecular basis of thermal stability from the analysis of ion pair networks in the glutamate dehydrogenase family. *Eur. J. Biochem.* 255: 336–346.